

# Spot the difference

## Impact of different selection criteria on early-type galaxies observed properties in zCOSMOS 20-k\* sample

M. Moresco<sup>1</sup>, L. Pozzetti<sup>2</sup>, A. Cimatti<sup>1</sup>, G. Zamorani<sup>2</sup>, M. Bolzonella<sup>2</sup>, F. Lamareille<sup>3</sup>, M. Mignoli<sup>2</sup>, E. Zucca<sup>2</sup>, S.J. Lilly<sup>4</sup>, C.M. Carollo<sup>4</sup>, T. Contini<sup>3,5</sup>, J.-P. Kneib<sup>6</sup>, O. Le Fèvre<sup>6</sup>, V. Mainieri<sup>7</sup>, A. Renzini<sup>8</sup>, M. Scodeggio<sup>9</sup>, S. Bardelli<sup>2</sup>, A. Bongiorno<sup>10</sup>, K. Caputi<sup>23</sup>, O. Cucciati<sup>2</sup>, S. de la Torre<sup>11</sup>, L. de Ravel<sup>11</sup>, P. Franzetti<sup>9</sup>, B. Garilli<sup>9</sup>, A. Iovino<sup>12</sup>, P. Kampczyk<sup>4</sup>, C. Knobel<sup>4</sup>, K. Kovač<sup>4</sup>, J.-F. Le Borgne<sup>3,5</sup>, V. Le Brun<sup>6</sup>, C. Maier<sup>4,24</sup>, R. Pello<sup>3,5</sup>, Y. Peng<sup>13</sup>, E. Perez-Montero<sup>3,5</sup>, V. Presotto<sup>12</sup>, J.D. Silverman<sup>14</sup>, M. Tanaka<sup>14</sup>, L. Tasca<sup>6</sup>, L. Tresse<sup>6</sup>, D. Vergani<sup>15</sup>, L. Barnes<sup>4</sup>, R. Bordoloi<sup>4</sup>, A. Cappi<sup>2</sup>, C. Diener<sup>4</sup>, A.M. Koekemoer<sup>13</sup>, E. Le Floch<sup>16</sup>, C. López-Sanjuan<sup>6,22</sup>, H.J. McCracken<sup>17</sup>, P. Nair<sup>2,13</sup>, P. Oesch<sup>4,18</sup>, C. Scarlata<sup>19</sup>, N. Scoville<sup>20</sup>, and N. Welikala<sup>21</sup>

(Affiliations can be found after the references)

Received – – –; accepted – – –

### ABSTRACT

**Aims.** We present the analysis of photometric, spectroscopic and morphological properties for differently selected samples of early-type galaxies up to  $z = 1$  extracted from the zCOSMOS-20k spectroscopic survey. This analysis intends to explore the dependence of galaxy properties on the selection criterion adopted, to study the degree of contamination due to star-forming outliers and to provide a comparison between different commonly used selection criteria. This work is a first step to fully investigate the early-type galaxies selection effects for future massive surveys such as Euclid.

**Methods.** We extracted from the zCOSMOS-20k catalog 6 different samples of early-type galaxies, based on morphology (2421 “morphological” early-type galaxies), optical colors (4894 “red-sequence” early-type galaxies and 4886 “UVJ” early-type galaxies), specific star formation rate (2937 “sSFR” early-type galaxies), a best-fit to the observed spectral energy distribution (2603 “photometric SED” early-type galaxies), and a criterion which combines morphological, spectroscopic and photometric informations (1530 “pure passive” early-type galaxies). We have studied for all the samples optical and infrared colors, morphological properties, specific star formation rates, and the equivalent widths of the residual emission lines; this analysis has been performed as a function of redshift and stellar mass, to inspect further possible dependencies.

**Results.** We find that each early-type galaxies sample displays a certain level of contamination due to blue/star-forming/non-passive outliers. The “morphological” sample is the one that presents the higher percentage of contamination, with  $\sim 20\text{--}70\%$  (depending on the mass range) of galaxies not located in the red-sequence,  $\sim 30\text{--}80\%$  of galaxies with a specific star formation rate  $\sim 30$  times higher than the adopted definition of “early-type”, and significant emission lines found in the median stacked spectra, at least for  $\log(\mathcal{M}/\mathcal{M}_\odot) < 10.25$ . The “pure passive” sample is the purest, with a percentage of contamination in color  $< 10\%$  for stellar masses  $\log(\mathcal{M}/\mathcal{M}_\odot) > 10.25$ , very limited tails in sSFR, and only up to a median value  $\sim 20\%$  higher than the chosen “early-type” cut, and equivalent widths of emission lines mostly compatible with no star formation activity; however, it is also the less economic criterion in terms of information used. Among the other criteria, we found that the best performing are the “photometric type” and the “sSFR”, providing a percentage of contamination only slightly higher than the “pure passive” criterion (on average of a factor of  $\sim 2$ ) but with absolute values of the properties of contaminants still compatible with a red, passively evolving population. We also find a strong dependence of the contamination on the stellar mass, and conclude that, almost irrespectively of the adopted selection criteria, a cut at  $\log(\mathcal{M}/\mathcal{M}_\odot) > 10.75$  provides a significantly purer sample in terms of star-forming contaminants. By studying the restframe color-mass and color-color diagrams we provided two revised definitions of early type galaxies based on these criteria, that better reproduce the observed bimodality in the properties of zCOSMOS-20k galaxies.

The analysis of the number densities of the various samples shows evidences of mass-assembly downsizing, with galaxies at  $10.25 < \log(\mathcal{M}/\mathcal{M}_\odot) < 10.75$  increasing their number by a factor  $\sim 2\text{--}4$  from  $z = 0.6$  to  $z = 0.2$ , by a factor  $\sim 2\text{--}3$  from  $z = 1$  to  $z = 0.2$  at  $10.75 < \log(\mathcal{M}/\mathcal{M}_\odot) < 11$ , and by only  $\sim 10\text{--}50\%$  from  $z = 1$  to  $z = 0.2$  at  $11 < \log(\mathcal{M}/\mathcal{M}_\odot) < 11.5$ .

**Key words.** galaxies: evolution – galaxies: fundamental parameters – galaxies: statistics – surveys

### 1. Introduction

Early-type galaxies (ETGs) represent a population of galaxies apparently simple and homogeneous in terms of morphology, colors, stellar population content and scaling relations (for a detailed review, see Renzini, 2006, and references therein), at least in the local Universe.

Send offprint requests to: Michele Moresco (e-mail: michele.moresco@unibo.it)

\* based on data obtained with the European Southern Observatory Very Large Telescope, Paranal, Chile, program 175.A-0839

Historically, these galaxies have been firstly identified morphologically, but it was soon evident that the morphological dichotomy between early-type (elliptical) and late-type (spiral) galaxies was rooted more deeply, and that it reflected an intrinsic difference between two distinct populations. It is now almost 50 years that is evident that galaxy rest-frame colors show a clear bimodal distribution, both in clusters (e.g. Visvanathan & Sandage, 1977; Tully et al., 1982) as in the field (Strateva et al., 2001; Hogg et al., 2002; Baldry et al., 2004a,b; Bell et al., 2004; Franzetti et al., 2007). Later studies have shown a bimodality also in many other galaxy parameters:  $H\alpha$  (Balogh et al., 2004) and [OII] (Mignoli et al., 2009) emission, 4000 Å break (Kauffmann et al., 2003), star formation history (Brinchmann et al., 2004), and clustering (Meneux et al., 2006). A similar bimodality has been found also in the galaxy stellar mass function, showing that early-type galaxies are the most massive galaxies at  $z \sim 0$  (Baldry et al., 2004a, 2006, 2008) and dominate the massive end of the stellar mass function up to  $z \sim 1$  (Pozzetti et al., 2010).

The properties of ETGs make them the ideal candidates to probe, together with galaxy formation models and theories, also cosmology. These galaxies have been found to have a stronger clustering with respect to late-type galaxies (e.g. see Zehavi et al., 2011, and references therein), providing a better tracer to the structure of underlying matter. This population of galaxies has been proposed also to be used as “cosmic chronometers”, able to trace the differential age evolution of the Universe as a function of redshift (Jimenez et al., 2002) and to provide independent and precise measurements of the Hubble parameter  $H(z)$  up to  $z \sim 1.5$  (Simon et al., 2005; Stern et al., 2010; Moresco et al., 2012a). This measurements have been demonstrated to be an innovative and complementary tool to constrain cosmological parameters (Moresco et al., 2011, 2012b; Wang et al., 2012; Riemer-Sørensen et al., 2013; Aviles et al., 2013; Said et al., 2013).

A powerful tool to study the evolution of a galaxy population is to analyze how evolves its number density as a function of redshift, since it can give ideas of the processes and characteristic time-scales involved. The number density of ETGs has been deeply studied by many authors, and there is a general agreement that, while there is a strong evolution for less massive galaxies, the number density of  $\log(M/M_\odot) > 11$  ETGs is almost unchanged from  $z \sim 1$  to  $z \sim 0$  (Scarlata et al., 2007; Pozzetti et al., 2010; Brammer et al., 2011; Maraston et al., 2012; Ilbert et al., 2013; Moustakas et al., 2013), and this has been interpreted as an evidence that this population of galaxy is already in place since  $z \sim 1$ .

From all these observational evidences, a formation and evolution scenario for this population of galaxies has been developed, for which early-type galaxies represent the reddest galaxy population, are the oldest among all galaxy types, they are often passively evolving and show also the strongest clustering, tending to inhabit the densest environments.

Based on this scenario, recently all these properties are often used without a clear distinction, and “red”, “quiescent”, and “old” are erroneously used as synonyms. Surely, as discussed above, the bimodality in many galaxy properties highlights that red galaxies are mostly quiescent and passively evolving; however, a detailed and quantitative es-

timate of the contamination due to blue/star-forming outliers should be made before doing a one to one correspondence. Franzetti et al. (2007) pointed out such possible contamination when studying a color-selected sample of ETGs, concluding that selecting galaxies only on the basis of their colors can be misleading in estimating the evolution of old and passively evolving galaxies.

In this paper, we want to extend this analysis, and study the effect of different ETGs selection criteria on their properties, and the level of contamination due to star-forming non-passive outliers. In Sect. 2 we will present our data, and how the different ETGs samples have been selected. In Sect. 3 the color, spectroscopic and morphological analysis will be presented. In Sect. 4 we will quantify how much each sample is contaminated by the presence of blue/star-forming outliers, and how this contamination depends on the stellar mass and on the adopted selection criterion. We will also analyze the number densities of the various samples, and compare them to check for differences and provide insights about the characteristic processes involved. Finally, we will also present two revised color-mass and color-color ETG selection criteria, aiming to reduce the contamination by blue star-forming galaxies.

This study will be interesting in the view of many upcoming surveys (e.g. Euclid, Laureijs et al., 2011), since it provides a comparison between different methods of selecting early-type galaxies, quantifying the purity of the sample as well as the cost in terms of information needed.

Throughout the paper, we adopt the cosmological parameters  $H_0 = 70 \text{ km s}^{-1} \text{ Mpc}^{-1}$ ,  $\Omega_m = 0.25$ ,  $\Omega_\Lambda = 0.75$ . Magnitudes are quoted in the AB system.

## 2. Data

### 2.1. The sample

The COSMOS Survey (Scoville et al., 2007) has imaged a field of  $\sim 2 \text{ deg}^2$  with the Advanced Camera for Surveys (ACS) with single-orbit I-band exposures to a depth  $I_{AB} \simeq 28 \text{ mag}$  and 50% completeness at  $I_{AB} = 26.0 \text{ mag}$  for sources  $0.5''$  in diameter (Koekemoer et al., 2007).

The analysis presented in this paper is based on the zCOSMOS spectroscopic survey (Lilly et al., 2007, 2009). This ESO Large Programme ( $\sim 600$  hours of observations) was aiming to map the COSMOS field with the Visible Multi-Object Spectrograph (VIMOS, Le Fèvre et al., 2003), mounted on the ESO Very Large Telescope (VLT). Our sample has been extracted from the zCOSMOS 20k bright sample (Lilly et al., 2009). The observed magnitudes in 12 photometric bands (CFHT  $u^*$ ,  $K$  and  $H$ , Subaru  $B_J$ ,  $V_J$ ,  $g^+$ ,  $r^+$ ,  $i^+$ , and  $z^+$ , UKIRT  $J$  and Spitzer IRAC at  $3.6 \mu\text{m}$  and  $4.5 \mu\text{m}$ ) have been used in order to derive reliable estimates of galaxy parameters from the photometric SED-fitting. The photometric catalog is described in (Capak et al., 2007). Following their approach, magnitudes were corrected for Galactic extinction using Table 11 of Capak et al. (2007) and the photometry was optimized by applying zeropoint offsets to the observed magnitudes to reduce differences between the observed and reference magnitudes computed from a set of template spectral energy distributions (SEDs). The spectra have been obtained using the VIMOS spectrograph mounted at the Melipal Unit Telescope of the VLT at ESO’s Cerro Paranal Observatory, with a medium resolution grism ( $R \approx 600$ )

with a slit width of 1 arcsec; the spectral ranges of the observations are typically 5550 – 9650 Å. The data have been reduced with VIMOS Interactive Pipeline Graphical Interface software (VIPGI, Scodreggio et al., 2005), and the redshift measured with EZ software (Garilli et al., 2010) with a high success rate ( $\approx 95\%$  in the redshift range  $0.5 < z < 0.8$ , Lilly et al., 2009). The lines measurements have been performed using the program *Platefit* (see Lamareille et al., 2006, for further details). After removing the spectroscopically confirmed stars, the broad-line AGNs, and the galaxies with an insecure redshift measurement ( $z_{\text{flag}} < 1.5$ ) we end up with a parent sample of 17431 galaxies.

The stellar masses ( $\mathcal{M}$ ) and Star Formation Rates (SFR) were estimated for the entire sample by performing a best fit to the SEDs, using the observed magnitudes in 12 photometric bands from  $u^*$  to  $4.5\mu\text{m}$ . A grid of theoretical models has been built from Bruzual & Charlot (2003) stellar population synthesis models (hereafter BC03), adopting an exponentially declining star formation history (SFH) with  $\tau = 0.1, 0.3, 0.6, 1, 2, 3, 5, 10, 15, 30$  Gyr, a Chabrier initial mass function (Chabrier, 2003), a solar stellar metallicity and a Calzetti extinction law (Calzetti et al., 2000) with  $0 < A_V < 3$ . Absolute magnitudes and colors were evaluated using the ALF software following the method described in Zucca et al. (2009). The specific Star Formation Rate (sSFR) has been defined as the ratio between the star formation rate and the stellar mass,  $\text{sSFR} = \text{SFR}/\mathcal{M}$ .

## 2.2. The selection criteria

Different selection criteria have been proposed so far to select early-type galaxies. This population is usually identified as spheroidal (E/S0) galaxies with old stellar population, no (or negligible) star formation, and a passive evolution as a function of cosmic time. We exploit here six different definitions, which are described below. These criteria have been chosen not to be too restrictive, because otherwise we would have a really bad completeness, but at the same time to minimize the contamination by blue, star-forming objects.

- **“morphological” ETGs.** The Zürich Estimator of Structural Types (ZEST; Scarlata et al., 2007) estimates the morphological type of galaxies with a combination of a principal component analysis (PCA) of five nonparametric diagnostics of galaxy structure (asymmetry, concentration, Gini coefficient, second-order moment of the brightest 20% galaxy pixels, and ellipticity) and of a parametric description of the galaxy light (the exponent of a single-Sérsic fit to the surface brightness distribution). This estimator has been applied to the full zCOSMOS-20k sample, providing morphological measurements for all the galaxies. Following this classification, we selected 2421 early-type (elliptical) galaxies matching an E morphology (Scarlata et al., 2007).
- **“UVJ” ETGs.** Following Williams et al. (2009), we extracted a sample of ETGs on the basis of a restframe color-color diagram, defined as:

$$(U - V)_{\text{rest}} > 0.88 \times (V - J)_{\text{rest}} + 0.69 \quad [0 < z < 0.5]$$

$$(U - V)_{\text{rest}} > 0.88 \times (V - J)_{\text{rest}} + 0.59 \quad [0.5 < z < 1]$$

with the additional constraints of  $(U - V)_{\text{rest}} > 1.3$  and  $(V - J)_{\text{rest}} < 1.6$ . With these cuts, we selected 4886 galaxies.

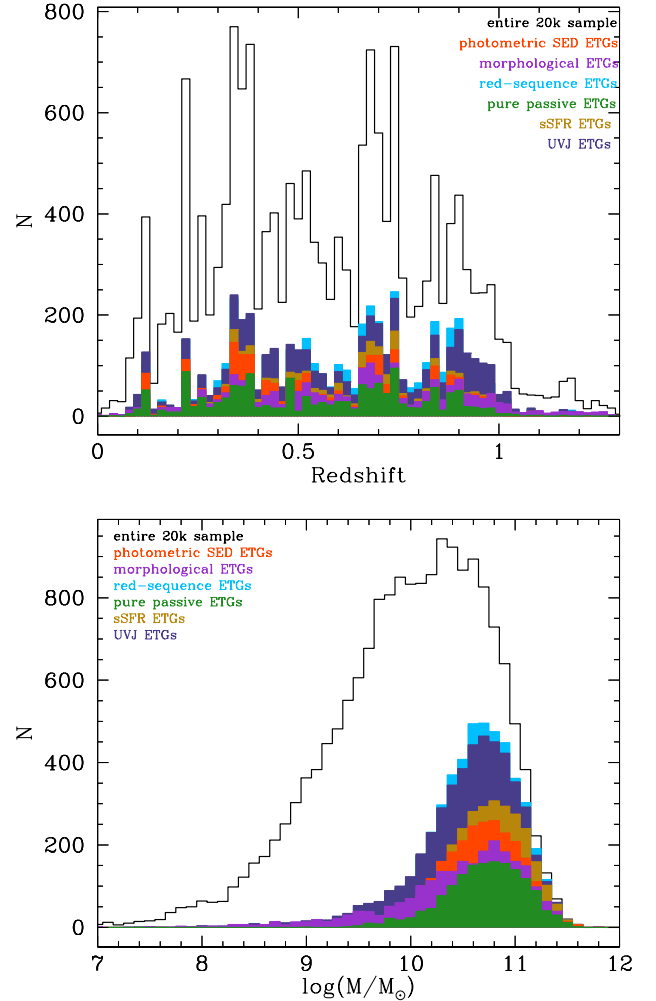


**Fig. 1.** Redshift distribution (upper panel) and stellar mass distribution (lower panel) of the entire zCOSMOS-20k sample, and of the different ETGs sample. In violet is shown the “morphological” ETGs, in blue the “UVJ” ETGs, in cyan the “red-sequence” ETGs, in yellow the “sSFR” ETGs, in orange the “photometric SED” ETGs, and in green the “pure passive” ETGs.

- **“photometric SED” ETGs.** Ilbert et al. (2009) employed a set of templates, generated by Polletta et al. (2007) with the code GRASIL (Silva et al., 1998), to fit the VIMOS VLT Deep Survey (VVDS) sources (Le Fèvre et al., 2005) from the UV-optical to the mid-IR. Therefore, this set of templates provides a better joining of UV and mid-IR than those previously proposed by (Ilbert et al., 2006). The nine galaxy templates of Polletta et al. (2007) include three SEDs of elliptical galaxies and six templates of spiral galaxies (S0, Sa, Sb, Sc, Sd, Sdm). Twelve additional templates obtained from BC03 models with starburst ages ranging from 3 to 0.03 Gyr are also added, to better represent the data. Finally, the templates were linearly interpolated, obtaining a total set of 32 templates. These templates were used to estimate photometric types from a best-fit to the observed photometry without additional dust extinction. With this method, we selected 2603 galaxies

best-fitted with an early-type template (i.e. SED-type from 1 to 8).

- **“red-sequence” ETGs.** In their analysis, Peng et al. (2010) defined a color-mass relation calibrated on SDSS and zCOSMOS-10k data, dividing red-sequence from blue-cloud galaxies. This relation takes also the redshift evolution into account and is a weak function of mass. Following their approach, 4894 red and passive galaxies have been selected on the basis of the following dividing rest-frame  $(U - B)$  color.

$$(U - B)_{\text{rest}} > 1.10 + 0.075 \times \log\left(\frac{\mathcal{M}}{10^{10} \mathcal{M}_{\odot}}\right) - 0.18 \times z$$

- **“sSFR” ETGs.** Following Ilbert et al. (2010) and Pozzetti et al. (2010), we selected 2937 quiescent galaxies on the basis of their specific Star Formation Rate, adopting the cut  $\log(\text{sSFR}) < -2$  [ $\text{Gyr}^{-1}$ ]. As shown by Ilbert et al. (2010), this cut corresponds almost directly to a cut  $(\text{NUV} - r_+)_{\text{template}} > 3.5$  with which they defined their sample of quiescent galaxies. With this selection criteria, we select galaxies which are increasing their mass at a rate less than 1/100th of their present mass.
- **“pure passive” ETGs.** To obtain a reliable sample, the less biased as possible for the presence of star-forming contaminants, we decided to follow the approach used in Moresco et al. (2010). From the parent sample, 1530 ETGs have been extracted by combining photometric, morphological and optical spectroscopic criteria: galaxies have been chosen with a best-fit to the SED matching a local E-S0 template (using the CWW templates of Ilbert et al., 2006), weak/no emission lines ( $\text{EW}_0([\text{OII}]/\text{H}\alpha) < 5$  Å), spheroidal morphology, and an observed  $(K - 24\mu\text{m})$  color typical of E/S0 local galaxies (i.e.  $(K - 24\mu\text{m}) < -0.5$ ); for further details about the sample selection, see Moresco et al. (2010).

Other standard definitions involve for example different set of templates to perform a best-fit match to the observed SED (CWW photometric types, Ilbert et al., 2006) or different cuts in the observed colors, as for the case of Luminous Red Galaxies (LRG, Eisenstein et al., 2001) and Baryon Oscillation Spectroscopic Survey (BOSS, Schlegel et al., 2009) samples. We checked, however, that the performances of these criteria are much worst than the ones of the other samples selected in our analysis in the selection of a pure sample of ETGs. In particular, LRGs and BOSS ETGs selections were optimized for the specific properties of those surveys, and can not straightforwardly be applied to zCOSMOS survey; we refer to Masters et al. (2011) for a discussion of the contamination by late-type morphological types of BOSS galaxies.

In Fig. 1 we show the redshift and mass distribution of the various ETGs samples. Each sample has been further divided into 6 subsamples, having considered separately two redshift ranges ( $z \leq 0.5$  and  $z > 0.5$ ) and three mass ranges (low-mass  $\log(\mathcal{M}/\mathcal{M}_{\odot}) < 10.25$ , medium-mass  $10.25 \leq \log(\mathcal{M}/\mathcal{M}_{\odot}) < 10.75$ , and high-mass  $\log(\mathcal{M}/\mathcal{M}_{\odot}) \geq 10.75$ ), to be able to discern the dependencies on mass and redshift.

In Tab. 1 we report the number of galaxies obtained with the different selections, as well as the percentage overlap between the various samples. As expected, the overlap

between samples obtained different selection criteria is often partial, suggesting that they have different properties. In particular, we notice that there is a small overlap between all samples and the morphologically-selected sample, indicating that a large fraction of ETGs selected on colors – or more generically on photometric properties – do not have an elliptical morphology (see Sect. 3.3). The overlap is also small when considering how many morphologically-selected ETGs are found in the other samples, indicating that a not-negligible fraction of ellipticals have blue colors. The overlap is, instead, larger when considering the other samples. The “red-sequence” and “UVJ” samples provide an almost identical number of galaxies, and show a similar reciprocal overlap of  $\sim 80\%$ ; however, as we will see in the following section, they have different photometric properties. The fraction of ETGs overlapping with the “red-sequence” sample is above  $\sim 80\%$  irrespectively of the selection criterion considered, but this is probably due to the higher number of galaxies of that sample. What is more interesting is to consider the fraction of ETGs included in the “sSFR” sample: the overlap with the “photometric SED” and the “pure passive” ETGs samples is above  $\sim 85\%$ , which testifies a quiescent star formation activity. Instead, for the “red-sequence” and the “UVJ” samples the overlap is  $\sim 60\%$ , indicating that almost half of that sample have a higher star formation activity. The last remark is about the “pure passive” criterion, which presents a small overlap with all the other samples: this is partly due to the smaller number of galaxies included in this sample, and partly because this is the only sample comprising also a spectroscopic cut (see Sect. 3.2).

### 3. The analysis

As already discussed, the early-type galaxies population is rather homogeneous in colors, star-formation activity and morphology. We therefore decided to inspect in details different properties, to study how their global properties change for the differently selected ETGs.

#### 3.1. Color properties

The primary observable, apart from the morphology, which we decided to examine is the color of the differently selected ETGs. We decided to study both the standard  $(U - B)_{\text{rest}}$  color-mass and  $(U - V)_{\text{rest}} - (V - J)_{\text{rest}}$  color-color plots, and an IRAC color-color diagram as firstly introduced by Lacy et al. (2004).

The  $(U - B)_{\text{rest}}$ -mass diagram is shown for both redshift ranges ( $z \leq 0.5$  and  $z > 0.5$ ) in Fig. 2. The gray hatched area represents the region which falls outside what is considered being the red-sequence, as defined by Peng et al. (2010) and previously reported. The clearest evidence is that most samples lie as expected in the red-sequence region; this is not surprising, since most selection criteria are based (or partially based) on an optical-color selection. For the morphologically selected ETGs, we found a confirmation of what deduced from Tab. 1, i.e. that this sample is contaminated by the presence of a not negligible tail of galaxies with blue  $(U - B)_{\text{rest}}$  colors ( $\sim 15\text{--}85\%$ ), both at high and low redshifts. Quite surprising is the tail of “UVJ” ETGs with blue color, which even forms a second peak in the  $(U - B)_{\text{rest}}$  distribution at  $z \leq 0.5$  (as shown in Fig. 2). This tails are due to the fact that the cut proposed

	morphology	UVJ	red-sequence	sSFR	photo-SED	pure passive	% w.r.t. global sample
morphology	<b>2421</b>	63.1%	60.0%	44.0%	39.7%	26.8%	13.9%
UVJ	30.6%	<b>4886</b>	83.3%	57.6%	49.8%	30.7%	28.1%
red-sequence	29.7%	83.2%	<b>4894</b>	59.2%	51.4%	31.0%	28.1%
sSFR	36.3%	95.8%	98.8%	<b>2937</b>	75.1%	47.0%	16.9%
photo-SED	37.0%	93.5%	96.6%	84.7%	<b>2603</b>	46.3%	14.9%
pure passive	41.5%	97.8%	99.2%	90.2%	78.8%	<b>1530</b>	8.8%

**Table 1.** ETGs samples overlap depending on the different selection criteria adopted, and number of galaxies (in boldface). Each box gives the percentage of galaxies of a particular sample (specified by the row’s name) found in another sample (specified by the column’s name). The last column reports also the percentage number of each sample with respect to the parent zCOSMOS-20k sample of 17431 galaxies.

by Williams et al. (2009) do not perfectly fit the observed bimodality in the UVJ diagram of the zCOSMOS-20k sample.

The  $(U - V)_{\text{rest}} - (V - J)_{\text{rest}}$  diagram provides a complementary information with respect to the color-mass diagram. As in the previous plot, we notice that the “pure passive”, the “sSFR”, and the “photometric SED” samples well fit the passive region defined by Williams et al. (2009) and identified by the non-hatched region of Fig. 3; we also observe as before the quite prominent tail of “morphological” ETGs with quite blue colors. Less expected is the fact that the “red-sequence” ETGs display a non negligible fraction of galaxies which do not fit perfectly the passive UVJ region. We will further discuss the issue of the different behavior of “red-sequence” and “UVJ” galaxies in Sect. 4.5.

The IRAC observed color-color plot is more interesting, since these colors less directly (or not at all) influence the various selection criteria, and are therefore a better indication of how much the samples are biased. As defined by Lacy et al. (2004), we plotted the  $8.0 \mu\text{m}/4.5 \mu\text{m}$  ratio against the  $5.8 \mu\text{m}/3.6 \mu\text{m}$  ratio in Fig. 4. This plot was initially introduced to identify AGN candidates, which should lie in the region identified by the dotted lines. More recently, Donley et al. (2012) revised this selection criteria to reduce the contamination by normal star-forming galaxies, by narrowing the region were the AGN candidates should lie (the area identified by the dashed lines). In their work, they also studied the predicted  $z = 0 - 3$  IRAC colors of different templates as a function of the AGN fraction, considering a star-forming template, a starburst, a normal star-forming spiral galaxy, and an elliptical galaxy. By analyzing the tracks of the elliptical galaxies, we found that they occupy a very specific region of the IRAC color-color diagram, i.e.  $\log(S_{8.0}/S_{4.5}) < -0.1 \cap \log(S_{5.8}/S_{3.6}) < -0.1$ , at least up to  $z \sim 2$ ; this region is indicated as the non-hatched region of Figure 4. From this plot it is evident that in both redshift ranges most of the samples are well located in a clump inside the region just defined; however, differently from the color diagrams, there are more pronounced tails outside this region. At  $z \leq 0.5$  almost all samples have show a very significant vertical tail with blue colors in  $S_{5.8}/S_{3.6}$  and red colors in  $S_{8.0}/S_{4.5}$ , which is a region in which low-redshift star-forming galaxies lie (for a comparison, see Fig. 2 of Donley et al., 2012). Differently, for  $z > 0.5$  the tails move toward red colors in both  $S_{5.8}/S_{3.6}$  and  $S_{8.0}/S_{4.5}$ . Even if they fall inside the AGN-candidates region defined by Lacy et al. (2004), it is very likely that most of these galaxies are higher-redshifts star-forming galaxies, as can be found following the tracks of Donley et al. (2012). On

the contrary, the morphologically selected ETGs display a clear tail exactly in the more restrictive AGN-candidate region of Donley et al. (2012), so it is likely that at least a fraction of these galaxies are actually AGN. This is confirmed also by the spectroscopic analysis (see Sect. 3.2), with spectra characterized by clear AGN features.

### 3.2. Spectroscopic properties

The spectroscopic properties of the galaxies have not been used (except in the “pure passive” criterion) to select ETGs: therefore they may provide interesting insights concerning the contamination of the various samples. We decided to look at the restframe equivalent widths of [OII] and H $\alpha$  lines, since they are well-known indicators of star formation activity. Given the wavelength coverage of zCOSMOS spectra, the two lines are not present in both redshift ranges: in particular H $\alpha$  line is observable at  $z \leq 0.5$ , while [OII] is observable at  $z > 0.5$ . These lines will be compared with another indicator of star formation, the sSFR, which provides the relative contribution of the star formation rate by weighting it with the total stellar mass of the galaxy.

Figure 5 shows  $\log(\text{sSFR}/\text{Gyr}^{-1})$  versus  $\text{EW}_0(\text{H}\alpha)$  (upper panel;  $z > 0.5$ ) and  $\text{EW}_0([\text{OII}])$  (lower panel;  $z \leq 0.5$ ). As expected, there exists a correlation (even if with a large dispersion) between the sSFR and the equivalent widths of [OII] and H $\alpha$  emission lines. Ilbert et al. (2010), aiming to study the galaxy stellar mass assembly by morphological and spectral type in the COSMOS field, identified as quiescent galaxies those with a dereddened color  $(\text{NUV} - r^+) > 3.5$ , and consequently a specific star formation rate  $\log(\text{sSFR}/\text{Gyr}^{-1}) < -2$ . Mignoli et al. (2009), analyzing the zCOSMOS sample, found that strong and weak line emitters can be well divided by an  $\text{EW}_0([\text{OII}]) = 5 \text{ \AA}$ . Combining these informations, we therefore identified  $\log(\text{sSFR}/\text{Gyr}^{-1}) < -2 \cap \text{EW}_0(\text{H}\alpha \text{ or } [\text{OII}]) < 5 \text{ \AA}$  as the region characteristic of early-type galaxies in this plot (the non-dashed area).

The “sSFR” and the “pure passive” ETGs samples present, by definition, no tail at high sSFR and EWs respectively. From the plot, we find that instead the color-selected samples (“UVJ” and “red-sequence”) and the “morphological” selected sample display a marked percentage of galaxies placed at both high sSFR and EWs, both at low and high redshifts. While it is not straightforward the interpretation of intermediate values of emission lines in terms of star formation (see for example Yan et al., 2006; Yan & Blanton, 2012), especially in the presence of a low level of sSFR, the concomitant higher level of sSFR clearly

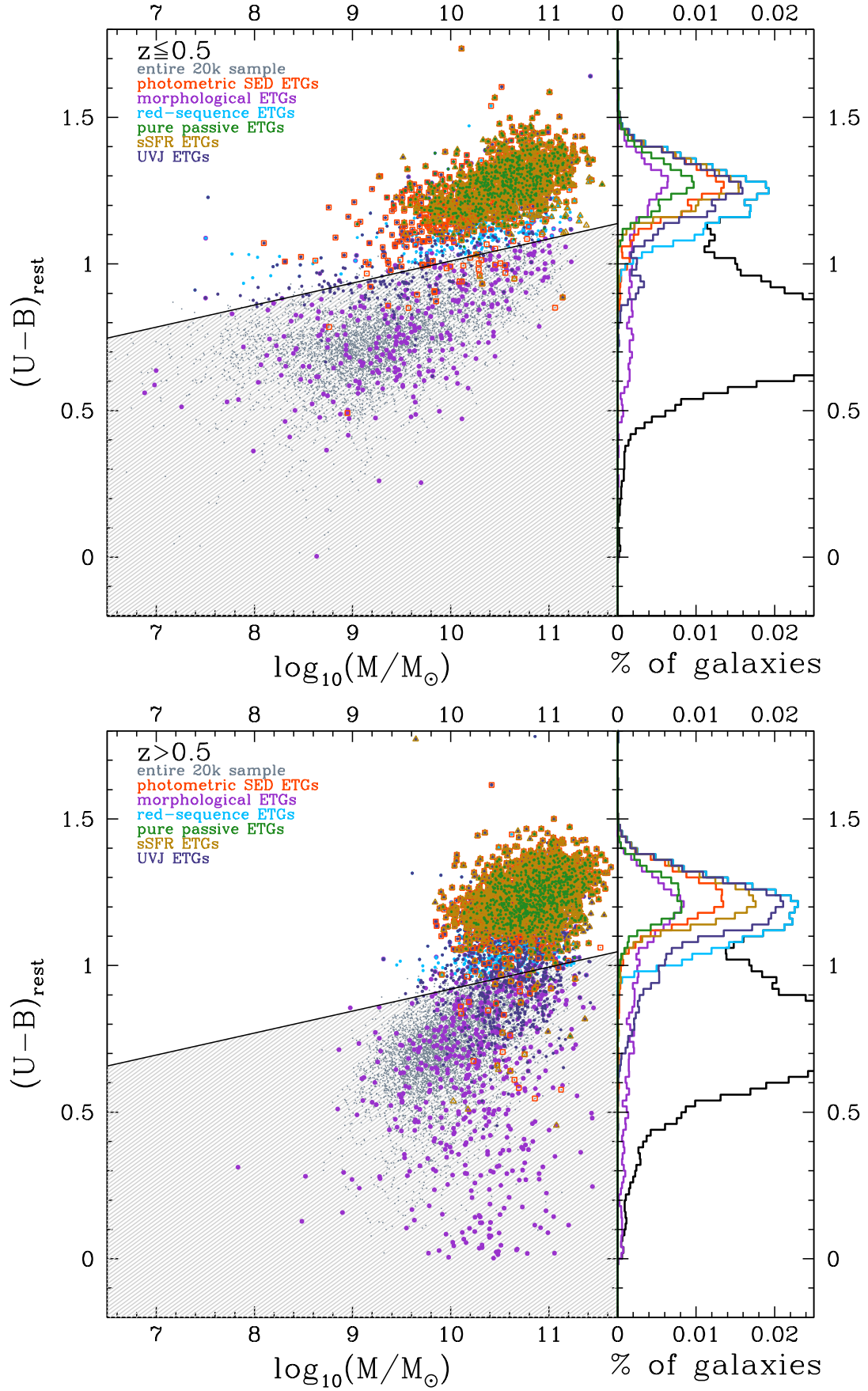


**Fig. 2.**  $(U-B)_{\text{rest}}$ -mass diagram. In gray the entire zCOSMOS-20k sample is shown, in violet the “morphological” ETGs, in blue the “UVJ” ETGs, in cyan the “red-sequence” ETGs, in yellow the “sSFR” ETGs, in orange the “photometric SED” ETGs, and in green the “pure passive” ETGs. The upper plot shows the  $(U-B)_{\text{rest}}$ -mass diagram obtained for  $z \leq 0.5$ , and the lower plot shows the diagram obtained for  $z > 0.5$ . The gray hatched area represent the region which falls outside the “passive” region of the  $(U-B)_{\text{rest}}$ -mass diagram, as defined in Sect. 2.2.



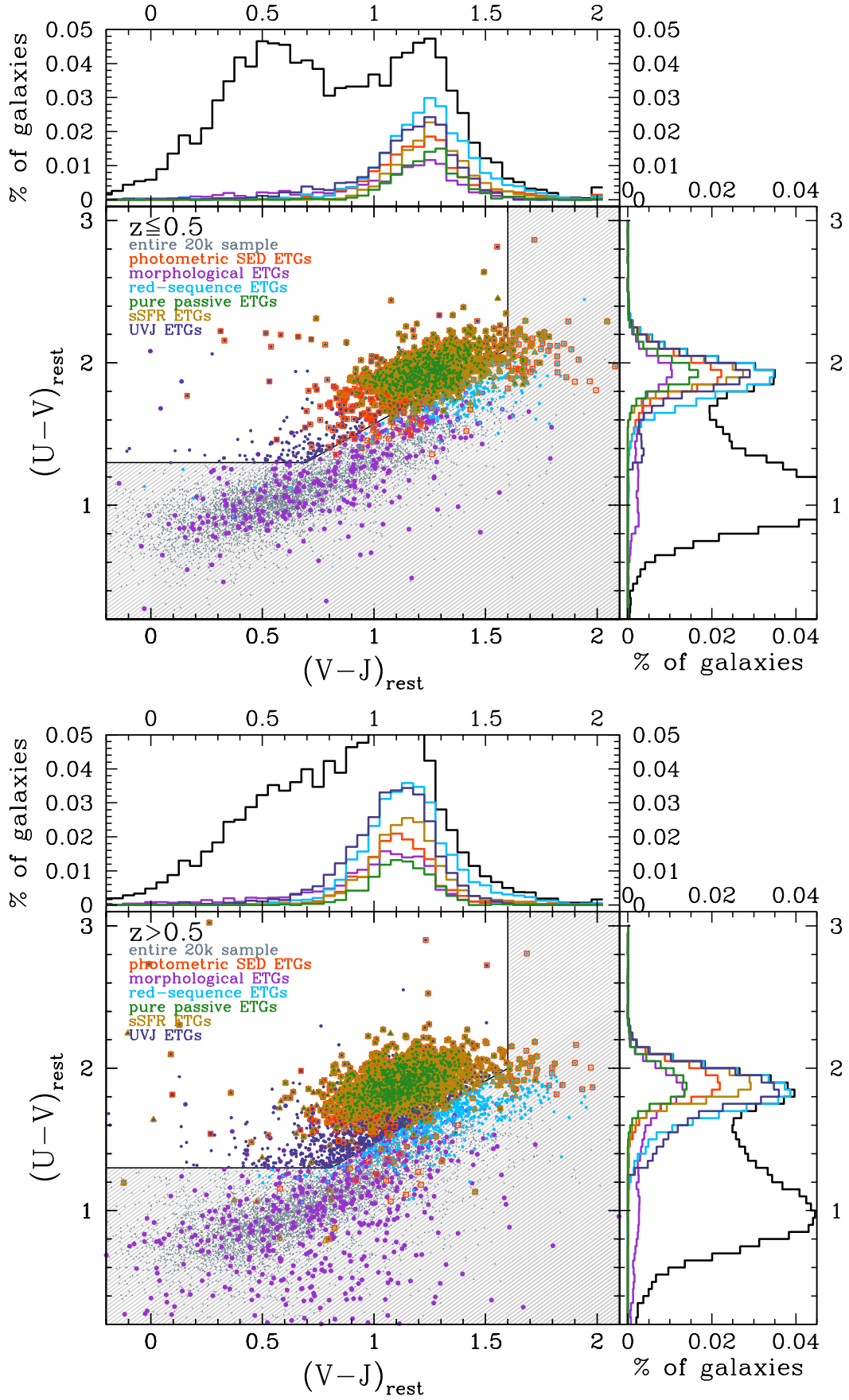


**Fig. 3.**  $(U - V)_{\text{rest}} - (V - J)_{\text{rest}}$  diagram. In gray the entire zCOSMOS-20k sample is shown, in violet the “morphological” ETGs, in blue the “UVJ” ETGs, in cyan the “red-sequence” ETGs, in yellow the “sSFR” ETGs, in orange the “photometric SED” ETGs, and in green the “pure passive” ETGs. The upper plot shows the diagram obtained for  $z \leq 0.5$ , and the lower plot for  $z > 0.5$ . The gray hatched area represent the region which falls outside the “passive” region of the UVJ diagram, as defined in Sect. 2.2.

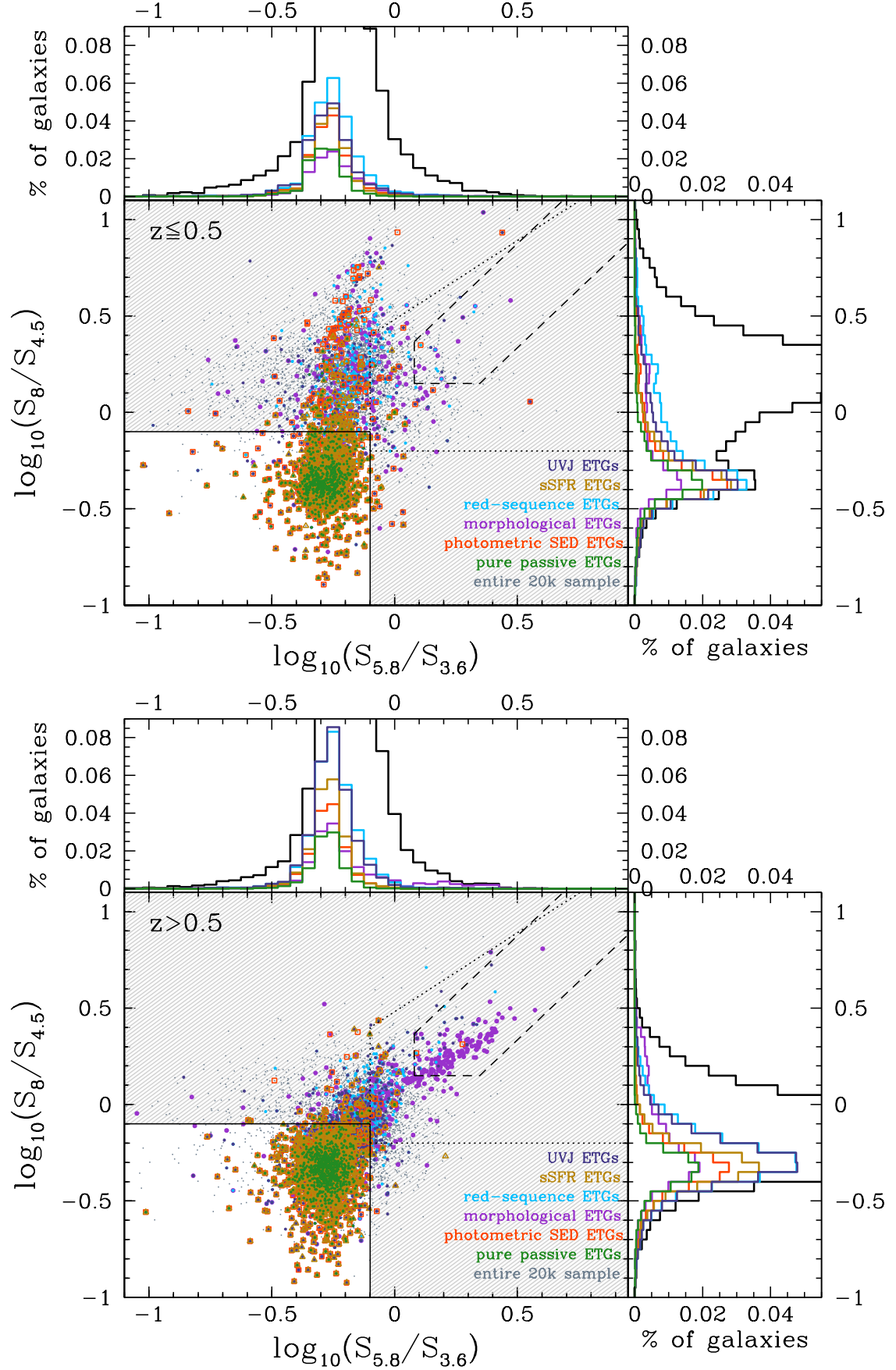


**Fig. 4.**  $\log(S_{8.0}/S_{4.5}) - \log(S_{5.8}/S_{3.6})$  diagram. In gray the entire zCOSMOS-20k sample is shown, in violet the “morphological” ETGs, in blue the “UVJ” ETGs, in cyan the “red-sequence” ETGs, in yellow the “sSFR” ETGs, in orange the “photometric SED” ETGs, and in green the “pure passive” ETGs. The upper plot shows the  $\log(S_{8.0}/S_{4.5}) - \log(S_{5.8}/S_{3.6})$  diagram obtained for  $z \leq 0.5$ , and the lower plot shows the diagram obtained for  $z > 0.5$ . The gray hatched area represent the region which falls outside the “passive” region of the IRAC color-color diagram, as defined in Sect. 3.1.



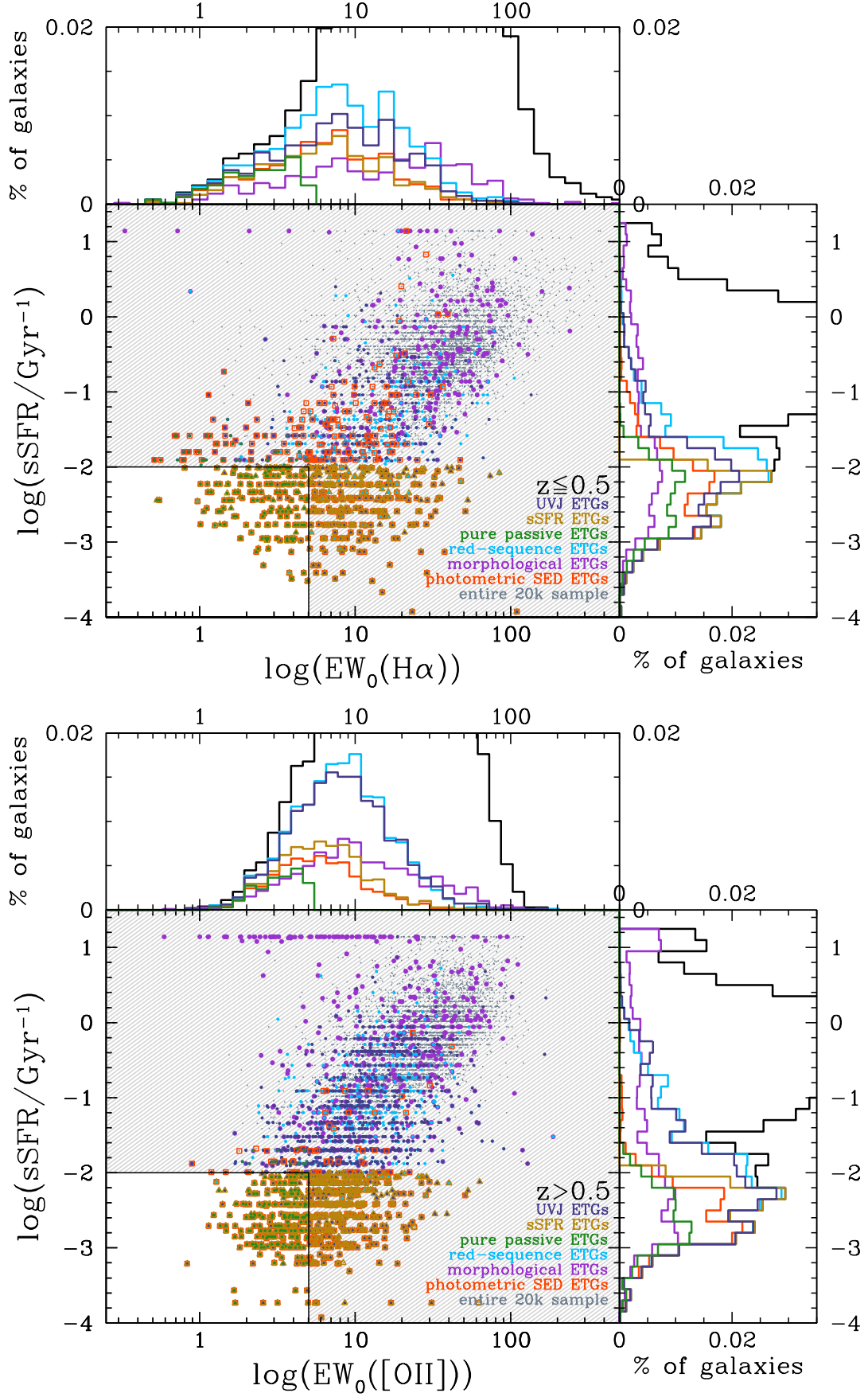


**Fig. 5.** sSFR- $\text{EW}_0([\text{OII}]/\text{H}\alpha)$  diagram. In gray the entire zCOSMOS-20k sample is shown, in violet the “morphological” ETGs, in blue the “UVJ” ETGs, in cyan the “red-sequence” ETGs, in yellow the “sSFR” ETGs, in orange the “photometric SED” ETGs, and in green the “pure passive” ETGs. The upper plot shows the sSFR- $\text{EW}_0(\text{H}\alpha)$  diagram obtained for  $z \leq 0.5$ , and the lower plot shows the sSFR- $\text{EW}_0([\text{OII}])$  diagram obtained for  $z > 0.5$ .

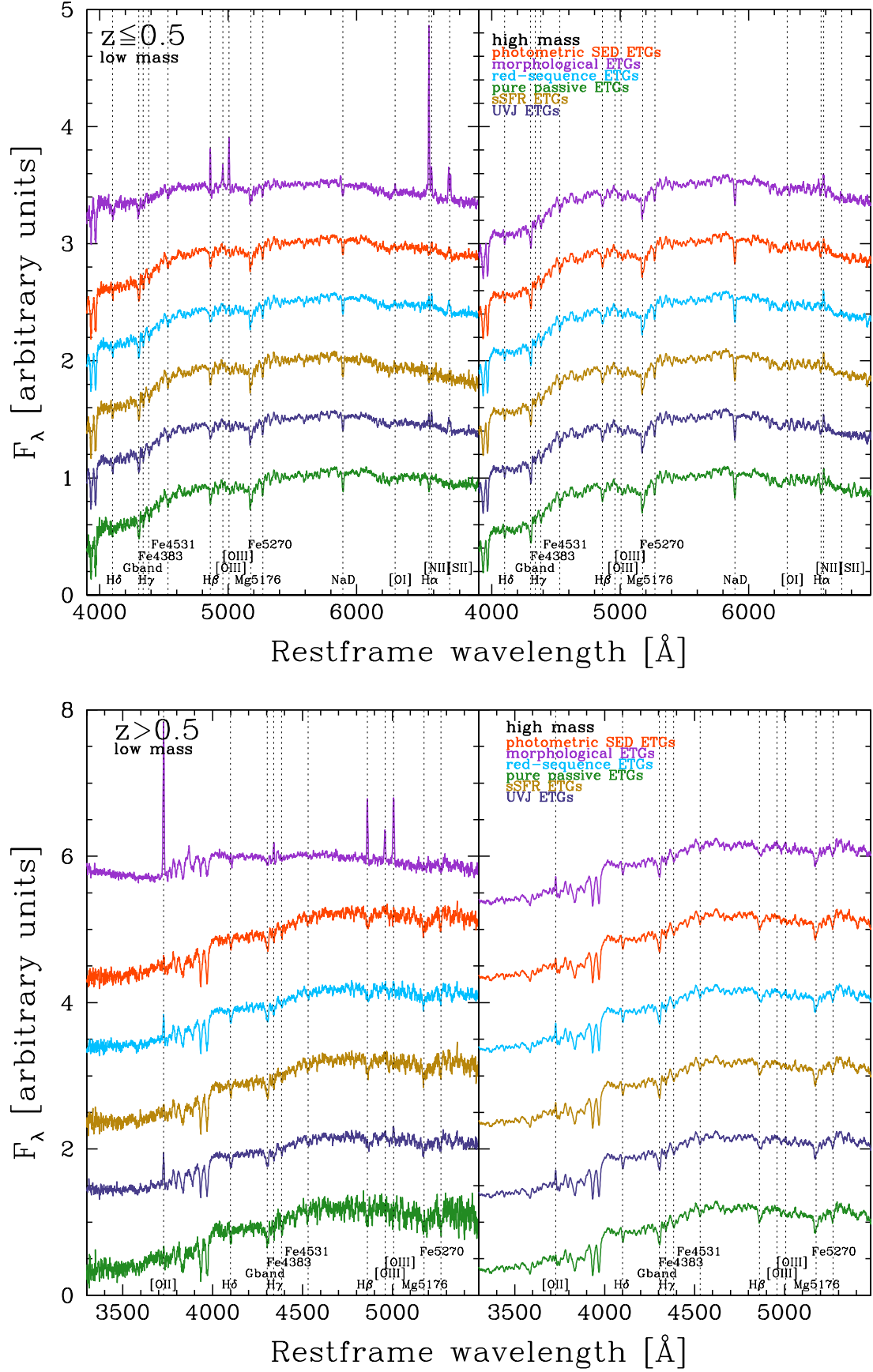


**Fig. 6.** Median stacked spectra obtained for  $z \leq 0.5$  (upper plot) and  $z > 0.5$  (lower plot); the spectra have been evaluated in the low-mass bin ( $\log(\mathcal{M}/\mathcal{M}_\odot) < 10.25$ , left panels) and in the high-mass bin ( $\log(\mathcal{M}/\mathcal{M}_\odot) > 10.75$ , right panels). In violet is shown the “morphological” ETGs, in blue the “UVJ” ETGs, in cyan the “red-sequence” ETGs, in yellow the “sSFR” ETGs, in orange the “photometric SED” ETGs, and in green the “pure passive” ETGs.

indicates a higher level of star formation with respect to the bulk of the population, which lies in the “early-type” region defined above.

We have also analyzed the stacked median spectra of all samples. In order to disentangle mass and redshift effects, in Fig. 6 we have plotted only the median spectra for the low- ( $\log(\mathcal{M}/\mathcal{M}_\odot) < 10.25$ ) and high-mass ( $\log(\mathcal{M}/\mathcal{M}_\odot) > 10.75$ ) subsamples, in the low- and high-redshift regimes. The “morphological” ETGs present the strongest emission lines, especially at low masses: at high redshift, strong emission lines in [OII], H $\beta$ , [OIII] are found; at low redshift, the measured ratios between [NII] $\lambda 6583$ /H $\alpha$  and [OIII] $\lambda 5007$ /H $\beta$  populate the star-forming region in the BPT diagram (Baldwin, Phillips & Terlevich, 1981), indicating a significant star formation in particular if we consider that we are analyzing median spectra (see also Pozzetti et al., 2010).

All the other samples show spectra with more typical passive continua, with the presence of faint emission lines in [OII] and H $\alpha$  only for the “UVJ” and “red-sequence” ETGs samples. At high masses, we find no traces of significant emission lines, and all the spectra show features and continua typical of passively evolving galaxies; this indicates a possible mass dependence that will be further analyzed in Sect. 4.2. In particular, we notice a small [OII] emission lines in most spectra at high redshifts, which, however, is compatible with not being caused by star formation activity (see Yan et al., 2006; Yan & Blanton, 2012, , and the discussion of Sect. 4.1). At low redshift, we note that all spectra present a detectable [NII] line (and often also [SII]), but no sign of H $\alpha$ , probably due to the fact that the H $\alpha$  emission line is hidden by the corresponding absorption line.

### 3.3. Morphological properties

To study in details the morphological properties of the differently selected ETGs, we have analyzed the ZEST (Scarlata et al., 2007) types of the various samples. While for almost all the samples a large fraction of galaxies have an E/S0 morphology (a clear example is shown in Fig. 7), there is however a significant fraction – which depends on the adopted selection criteria – of galaxies with clearly spiral/irregular morphologies (see Fig. 8). The fact that all the samples are contaminated by late-type morphologies is a consequence of the fact that even if it is evident the correspondence between the bimodality in photometric properties and in morphological types, the color and the morphological transformation are two distinct processes taking place at different times in the life of a galaxies.

This result confirms what found with independent methods by other analyses (e.g. see Pozzetti et al., 2010; Ilbert et al., 2010), i.e. that the morphological transformation from late-type to early-type galaxies is a process which intervenes on different time-scales than the color transformation, so that it is likely for a galaxy, even if it has already stopped its star formation activity, still not to have an elliptical morphology. Therefore, differently from other properties, it is improper to consider those galaxies as star-forming contaminant, and the presence of morphologically late-type galaxies will be considered separately.

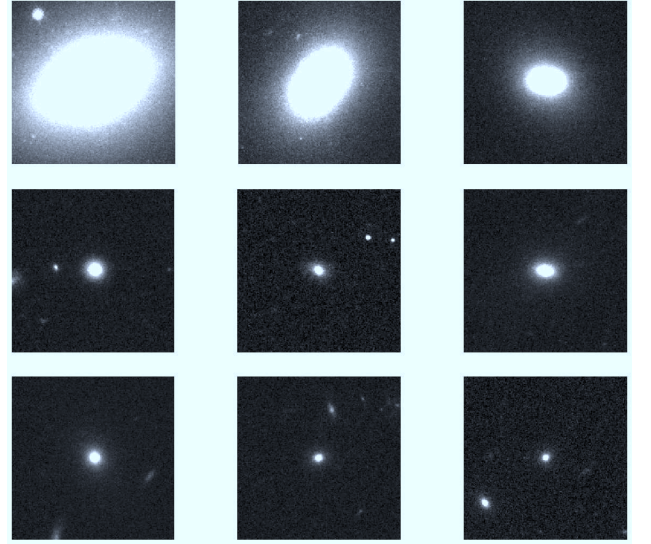


**Fig. 7.** Examples of ACS morphology for a subsample of the “pure passive” ETGs with elliptical morphologies. The galaxies are shown at increasing redshift from upper-left to lower-right, from  $z = 0.0791$  to  $z = 0.9302$ .

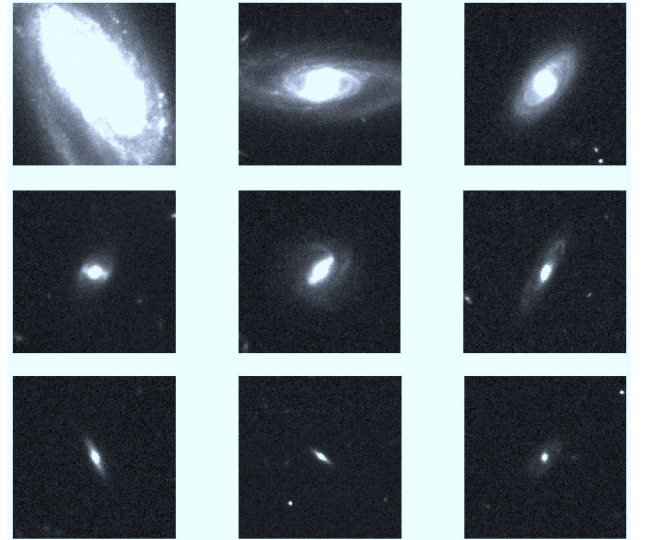


**Fig. 8.** Examples of ACS morphology for a subsample of the “pure passive” ETGs with very late-type morphologies, found for less than 10% of the overall sample. The galaxies are shown at increasing redshift from upper-left to lower-right, from  $z = 0.0998$  to  $z = 0.834$ .

## 4. Results

To estimate which criterion is better in defining an ETGs sample the less biased as possible, we estimated the level of contamination by examining different observables, considering colors, sSFR, spectroscopic features and visual morphology. Of course, as anticipated before, these criteria should not to be too restrictive, because otherwise we will trade purity for a really bad completeness.

By definition, the less contaminated criterion will be the “pure passive”, using all the possible information available

for these galaxies. However, in the context of many galaxy surveys, it is of utmost interest also to identify a sample which is at the same time the most economic as possible (in terms of information used) and less biased as possible (in terms of star-forming outliers). To carry on this analysis, it will be necessary not only to consider the percentage of contaminants present in each sample, but also their absolute values, and the dependence on the redshift and on the stellar mass of the contamination.

#### 4.1. Study of the contamination

The criteria adopted to define a contaminant are complementary to the ones used to select the various ETGs samples, and are described below:

- *blue*  $(U - B)_{\text{rest}}$  colors:

$$(U - B)_{\text{rest}} < 1.10 + 0.075 \log\left(\frac{M}{10^{10} M_{\odot}}\right) - 0.18 z$$

- *non passive UVJ* colors:

$$(U - V)_{\text{rest}} < 0.88 \times (V - J)_{\text{rest}} + 0.69 \quad [+0.59 \text{ for } z > 0.5]$$

$$\cup (U - V)_{\text{rest}} < 1.3 \quad \cup (V - J)_{\text{rest}} > 1.6$$

- *high sSFR*:

$$\log(\text{sSFR}) > -2 \text{ [Gyr}^{-1}\text{]}$$

- *non passive IRAC* colors:

$$\log(S_{8.0}/S_{4.5}) > -0.1$$

$$\cup \log(S_{5.8}/S_{3.6}) > -0.1$$

- *presence of emission lines*:

$$\text{EW}_0(\text{H}\alpha) > 5 \text{ \AA} \text{ (if } z \leq 0.5\text{)} \\ \text{or } \text{EW}_0([\text{OII}]) > 5 \text{ \AA} \text{ (if } z > 0.5\text{)}$$

- *non-elliptical morphology*: ZEST type later than E.

For each mass- and redshift-subsample of the various ETGs samples defined in Sect. 2.2, we estimated the median  $(U - B)_{\text{rest}}$  color, sSFR, IRAC colors, restframe equivalent width of  $\text{H}\alpha$  ( $[\text{OII}]$  for  $z > 0.5$ ) and morphology of the just defined *contaminant*, and the percentage of contamination relative to each subsample. These values are reported in Tab. 2.

As discussed above for the morphology, also the spectroscopic properties would be worth a dedicated discussion, since it is not straightforward that a weak  $[\text{OII}]$  or  $\text{H}\alpha$  emission line is symptomatic of star-formation activity (Yan et al., 2006; Yan & Blanton, 2012). However, for simplicity we will address as contaminant a galaxy having any of these properties considered non standard for an early type, and examine each one individually.

For each considered property, it is evident for all the samples a trend with stellar mass, with a decreasing percentage of contaminants with increasing mass; this effect will be analyzed in the following section. Below we discuss separately the contamination in optical and IRAC colors, in sSFR, in spectroscopy, and in morphology.

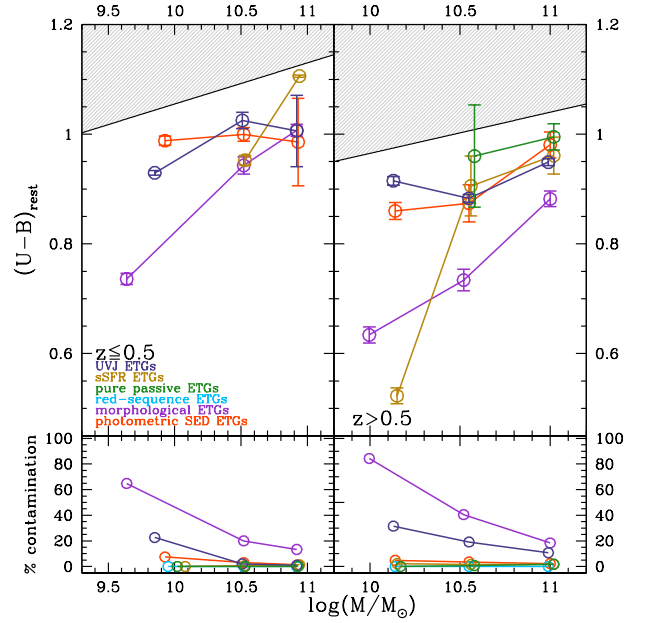


**Fig. 9.** Median  $(U - B)_{\text{rest}}$  color (upper panel) and relative percentage (lower panel) as a function of stellar mass of galaxies with blue colors, i.e.  $(U - B)_{\text{rest}} < 1.10 + 0.075 \log\left(\frac{M}{10^{10} M_{\odot}}\right) - 0.18 z$ , for the different selection criteria (in violet the “morphological” ETGs, in orange the “photometric SED” ETGs, in cyan the “red-sequence” ETGs, in yellow the “sSFR” ETGs, in blue the “UVJ” ETGs, and in green the “pure passive” ETGs). The errorbars represent the error on the median.

**Blue  $(U - B)_{\text{rest}}$  colors.** In Sect. 3.1 we have shown the  $(U - B)_{\text{rest}}$ -mass diagram for all the samples, proving that, given the adopted selection criteria, almost all the selected ETGs lie in the red-sequence, with minor tails extending in the blue-cloud. As a consequence, the number of outliers with clearly blue colors are a minor percentage, typically  $\lesssim 5\%$  for all criteria (except “morphological” and “UVJ” ETGs) both at low and high redshift; moreover, as can be inferred by Tab. 2, this small fraction of blue outliers have relatively red colors, very close to the considered separation between red-sequence and blue-cloud. On the contrary, “morphological” ETGs display a substantial percentage of galaxies –  $\sim 20 - 80\%$  depending on the redshift range and on the mass regime – with a median  $(U - B)_{\text{rest}}$  color bluer with respect to the contaminants present in the other samples. This fact testifies that even if it exists a correlation between photometric properties and morphology of passive galaxies, this is not a one-to-one correlation, and a considerable number of blue ellipticals coexist with their more standard red counterparts (see also Tasca et al., 2009). Also the “UVJ” ETG sample present a significant contamination,  $\sim 30\text{--}10\%$  depending on the redshift range and on the mass regime; this is probably due to the fact that the color cuts defined by Williams et al. (2009) do not seem to reproduce well the observed bimodality in the UVJ diagram (as it can be seen by Fig. 3), with in particular evident tails in the blue part of the  $(U - V)_{\text{rest}}$  histogram. However, the median color of the contaminant is, as in most of the previous



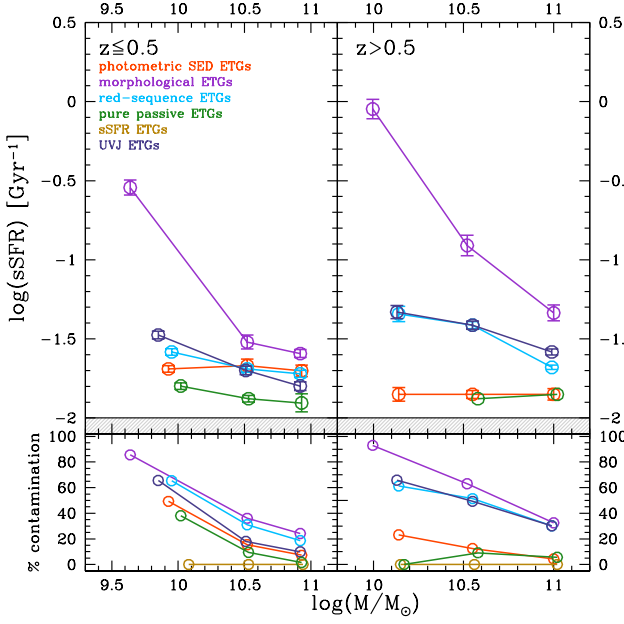


**Fig. 10.** Median  $\log(\text{sSFR}/\text{Gyr}^{-1})$  (upper panel) and relative percentage (lower panel) as a function of stellar mass of galaxies with high sSFR, i.e.  $\log(\text{sSFR}/\text{Gyr}^{-1}) > -2$ , for the different selection criteria (In violet the “morphological” ETGs, in blue the “UVJ” ETGs, in cyan the “red-sequence” ETGs, in yellow the “sSFR” ETGs, in orange the “photometric SED” ETGs, and in green the “pure passive” ETGs). The errorbars represent the error on the median.

cases, very close to the adopted definition of red-sequence. All these data are reported in Tab. 2 and shown in Fig. 9.

**Non passive UVJ colors.** For the UVJ color-color diagram, we considered a contaminant a galaxy with  $(U - V)_{\text{rest}}$  and  $(V - J)_{\text{rest}}$  colors outside the region defined by Williams et al. (2009). Therefore we just estimated the percentage of these galaxies for each selection criterion, and refer to Sect. 3.1 for the discussion about where those contaminants lie in the UVJ color-color diagram.

This analysis confirms the results just discussed for the color-mass diagram: the “sSFR”, “photometric SED” and “pure passive” ETGs fit almost perfectly to the passive region in the UVJ diagram, with a percentage of contaminants always below 20% at low redshift and below 5% at high redshift. The percentage of contaminants is slightly higher for the “red-sequence sample”, around 10-30%, and this fact demonstrate that also the cut defined by Peng et al. (2010) in the  $(U - B)_{\text{rest}}$  is not optimal in dividing passive and star-forming galaxies. As in the previous analysis, the “morphological” ETGs are the sample with the highest contamination in UVJ colors, around 20-80% depending on the redshift and mass ranges.

**High sSFR.** Considering the specific star formation rates, the “morphological” ETGs are the sample with the most extended tails ( $\sim 30\text{-}90\%$ ), with median values up to  $\log(\text{sSFR}/\text{Gyr}^{-1}) \sim -0.5$ , corresponding to a star formation activity  $\sim 30$  times higher with respect to the adopted

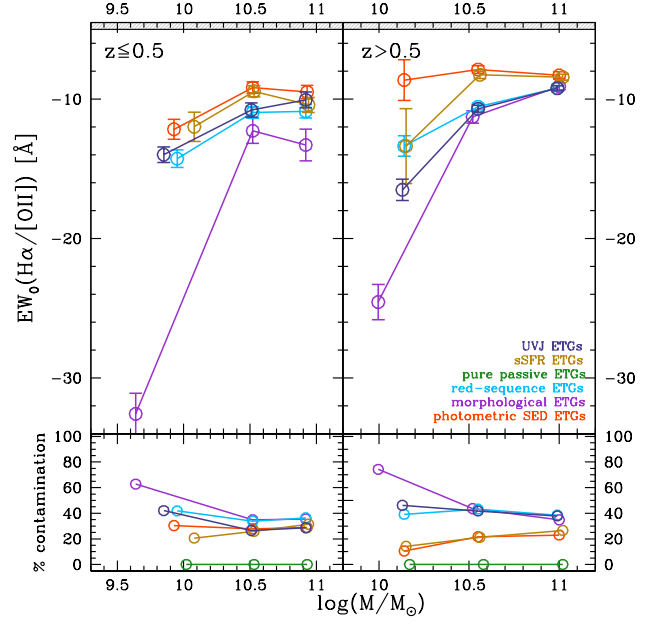


**Fig. 11.** Median  $\text{EW}_0(\text{H}\alpha)$  (upper panel;  $\text{EW}_0([\text{OII}])$  if  $z > 0.5$ ) and relative percentage (lower panel) as a function of stellar mass of galaxies with significant emission lines, i.e.  $\text{EW}_0(\text{H}\alpha) > 5 \text{ \AA}$  (if  $z \leq 0.5$ ) and  $\text{EW}_0([\text{OII}]) > 5 \text{ \AA}$  (if  $z > 0.5$ ), for the different selection criteria (In violet the “morphological” ETGs, in blue the “UVJ” ETGs, in cyan the “red-sequence” ETGs, in yellow the “sSFR” ETGs, in orange the “photometric SED” ETGs, and in green the “pure passive” ETGs). The errorbars represent the error on the median. By convention, the emission lines are quoted with negative values.

definition of quiescent (i.e.  $\log(\text{sSFR}/\text{Gyr}^{-1}) < -2$ ). Both “UVJ” and “red-sequence” samples represent an intermediate case, with a median  $\log(\text{sSFR}/\text{Gyr}^{-1}) \sim -1.5/-1.7$  for the contaminants ( $\sim 3$  times more star formation activity than the assumed quiescent limit), and a percentage of contamination  $\sim 20\text{-}65\%$ , depending on the mass range. The less biased sample (the “sSFR” sample is by definition not biased with respect to this parameter) are the “photometric SED” and the “pure passive” ETGs samples, having median values of sSFR much closer to the quiescent limit, and percentage of contamination in most cases  $\lesssim 15\%$ . All these data are reported in Tab. 2 and shown in Fig. 10.

**Non passive IRAC colors.** The study of the IRAC colors allows a clearer estimate of the presence of star-forming contaminants, since these bands were not directly used to define ETGs samples (they were used in the “photometric SED” ETGs, but together with all the other photometric bands for the best-fit to the SEDs). We considered as a contaminant a galaxy falling outside the “early-type IRAC selection” defined in Sect. 3.1. Therefore, since it is possible for such galaxy to have a redder  $S_{5.8}/S_{3.6}$  color, or a redder  $S_{8.0}/S_{4.5}$  color, or both, as for the UVJ case we just estimated the percentage of these galaxies for each selection criterion, and refer to Sect. 3.1 for the discussion about where those contaminants lie in the IRAC color-color diagram.

The “morphological” ETGs are the sample with the higher percentage of contamination,  $\sim 20\text{--}75\%$  as a function of mass independently of the redshift range. Similarly to the case of the sSFR, the “UVJ” and the “red-sequence” ETGs result to be more biased, with  $\sim 25\text{--}55\%$  (depending on the mass range) of the sample not classified as early-type for the IRAC color-color criterion at  $z \leq 0.5$  and  $\sim 10\text{--}50\%$  at  $z > 0.5$ . Apart from the “pure passive” sample, with a contamination of  $\sim 5\text{--}25\%$  at low redshift and of  $\sim 2\text{--}40\%$  at high redshift (from the lowest to the highest masses), the purest samples are the “sSFR” and the “photometric SED” ETGs ( $\sim 10\text{--}45\%$  at low redshift and  $\sim 3\text{--}45\%$  at high redshift).

**Presence of emission lines.** We have estimated the median equivalent width of  $\text{H}\alpha$  at  $z \leq 0.5$ , and  $[\text{OII}]$  at  $z > 0.5$  for the galaxies with significant emission lines (i.e.  $> 5 \text{ \AA}$ ) in each sample, and the results are reported in Tab 2 and shown in Fig. 11. The sample with the strongest emission lines is the “morphological” ETGs, with median equivalent widths up to  $\sim 30 \text{ \AA}$  and with a percentage of contamination going from 60-70% to 35%, depending on the mass range. The “UVJ” and the “red-sequence” samples show a similar and smaller contamination both in percentage ( $\sim 40\%$ ) and median value ( $\sim 15\text{--}10 \text{ \AA}$ ). The less contaminated samples are the “sSFR” and the “photometric SED” ETGs: the percentage of galaxies with emission lines  $> 5 \text{ \AA}$  is  $\sim 30\%$  at low redshift and slightly smaller ( $\sim 20\%$ ) at higher redshift, with median values closer to the adopted cut ( $\sim 8\text{--}10 \text{ \AA}$ ).

Many works have already shown the presence of emission lines in ETGs spectra. However, given their line ratios, these are usually classified as LINERS (Low-Ionization Nuclear Emission-line Regions, Heckman, 1980), or with a LINER-like emission (e.g. see Phillips et al., 1986; Yan et al., 2006; Annibali et al., 2010; Yan & Blanton, 2012). As summarized by Annibali et al. (2010), the most probable mechanisms proposed to produce such lines are a low accretion-rate AGN, fast shocks, or photoionization by old post-asymptotic giant branch (PAGB) stars. More recent studies favor the last option (see also Yan & Blanton, 2012). It is beyond the aim of this paper to analyze in detail the source of ionization in ETGs; what we wanted to stress here is that in this population of galaxies weak emission lines do not necessarily trace star formation activity, especially if the sSFR as found from the SED-fitting does not confirm a significant star formation. On the other hand, the stronger emission lines found in “morphological” ETGs should actually trace a star formation activity, as confirmed by the ratio with the other significant emission lines ( $\text{H}\beta$ ,  $[\text{NII}]\lambda 6583$ ,  $[\text{OII}]\lambda 5007$ ).

**Non-elliptical morphology.** The median morphology estimated for the galaxies not matching an elliptical template is equal to a ZEST type = 2.1, corresponding to a bulge-dominated spiral galaxy, in all samples. This means that for all ETGs samples the tail of morphologies is not extended toward very late-type templates. However, all the samples show a high percentage of contamination due to non elliptical galaxies, with percentages going from  $\sim 60\%$  at low masses to  $\sim 25\text{--}30\%$  at high masses, the less biased sample being the “pure passive” one.

This evidence is a confirmation that the color transformation and the morphological transformation from late-type to early-type galaxies are not concomitant processes, but the quenching of the star formation activity precedes the change in morphology.

#### 4.2. Contamination as a function of mass

The analysis of the different properties of ETGs has pointed out a clearly evident dependence of the contamination on the stellar mass. Looking at Tab. 2 it is possible to see that the percentage of contamination in almost all the analyzed properties decreases from  $\log(\mathcal{M}/\mathcal{M}_\odot) < 10.25$  to  $\log(\mathcal{M}/\mathcal{M}_\odot) > 10.75$  by a factor  $\sim 2\text{--}3$ . Figures 9, 10, and 11 highlight also a mass dependence of the absolute value of the properties of the contaminants in all samples: for example the colors of contaminants are redder by  $\sim 10\text{--}30\%$  at high masses than at low masses, and closer to the red-sequence. This trend can be found also in sSFR and equivalent widths of emission lines, with the lower mass bin having a star formation activity  $\sim 10\%$  higher and emission lines  $\sim 5 \text{ \AA}$  larger than the high mass bin for all the samples considered, both at high and at low redshift.

From this analysis we found that, irrespectively of the adopted ETG selection criterion, an additional stellar mass cut provides a purer sample in terms of star-forming contaminants.

#### 4.3. Contamination as a function of selection criteria

There are different ways to quantify which is the best method to select early-type galaxies: on one hand it is possible to ask which is the criterion least biased by the presence of star-forming outliers, independently of how much information is used; on the other hand, at a fixed percentage of contamination, it is possible to ask which is the most economic criterion in terms of information used. The first will privilege the purity of the sample, but has the drawback of requiring a large amount of data to be used; the second, on the contrary, will be necessarily more contaminated, but also of greatest interest in many surveys where, due to a low spectral resolution or to a limited wavelength coverage, less data are available.

Needless to say, the purest sample is the one based on the combined selection criterion, since the use of photometric, spectroscopic and morphological information helps to minimize the presence of blue, star-forming galaxies. It provides red and passive galaxies with a color contamination, also in the IRAC colors,  $< 10\%$  for stellar masses  $\log(\mathcal{M}/\mathcal{M}_\odot) > 10.25$ , both at low and high-redshifts. The specific star formation of the outliers ( $\lesssim 10\%$  for  $\log(\mathcal{M}/\mathcal{M}_\odot) > 10.25$ ) is only  $\sim 20\%$  higher than the chosen “early-type” cut, and the contaminants equivalent widths of emission lines, both  $[\text{OII}]$  and  $\text{H}\alpha$  are smaller than  $\sim 10 \text{ \AA}$ .

Apart from this criterion, all the others, except the morphological criterion, are equivalent in terms of requirements, since they all require a best fit to the observed SED to obtain stellar masses, SFRs and/or restframe colors needed to perform the selection. Among them, the best-performing criteria have proven to be the “photometric SED” and the “sSFR” ones. The analysis of Tab. 2 and Figs. 9, 10, and 11 shows that they have the minimum



	$z \leq 0.5$						$z > 0.5$					
	low-mass		med-mass		high-mass		low-mass		med-mass		high-mass	
	median	%	median	%	median	%	median	%	median	%	median	%
<b>blue <math>(U - B)_{\text{rest}}</math> colors</b>												
morphology	0.74	64.8%	0.94	20%	1.01	13.3%	0.63	84.3%	0.72	41.6%	0.77	22.8%
UVJ	0.93	22.6%	1.03	2%	1.01	0.9%	0.91	31.5%	0.88	19.2%	0.95	10.8%
red-sequence	–	–	–	–	–	–	–	–	–	–	–	–
sSFR	–	0.0%	0.95	0.8%	1.11	1.3%	0.52	2.2%	0.91	1.6%	0.96	1.7%
photo-SED	0.99	7.5%	1.00	3%	0.98	1.3%	0.86	4.8%	0.87	3.6%	0.98	2.3%
pure passive	–	0.0%	–	0.0%	–	0.0%	–	0.0%	0.96	0.7%	1	1.8%
<b>non passive UVJ colors</b>												
morphology	64.3%		29.8%		25.6%		82.9%		38.6%		17.5%	
UVJ	–		–		–		–		–		–	
red-sequence	23.1%		28.2%		29.5%		23.3%		24.3%		12.7%	
sSFR	1.4%		13.6%		22.2%		3.3%		3.7%		3.6%	
photo-SED	8.9%		16.5%		18.2%		5.8%		5.6%		4.6%	
pure passive	3.9%		13.2%		10.8%		0.0%		1.1%		1.5%	
<b>high sSFR</b>												
morphology	-0.54	85.6%	-1.52	36.1%	-1.59	24.1%	-0.05	93.0%	-0.86	63.7%	-1.15	36.4%
UVJ	-1.48	65.6%	-1.70	18%	-1.80	9.9%	-1.3	65.8%	-1.41	49.3%	-1.58	30.1%
red-sequence	-1.58	65.4%	-1.69	31.1%	-1.72	18.7%	-1.34	61.2%	-1.41	51.4%	-1.68	30.3%
sSFR	–	–	–	–	–	–	–	–	–	–	–	–
photo-SED	-1.69	49.3%	-1.67	15.4%	-1.70	7.2%	-1.85	12.4%	-1.85	13.2%	-1.85	4.4%
pure passive	-1.80	38.1%	-1.88	9.5%	-1.91	1.6%	–	0.0%	-1.88	9.1%	-1.85	5.6%
<b>non passive IRAC colors</b>												
morphology	71.4%		27.5%		20.2%		74.7%		37.3%		20.4%	
UVJ	55.2%		13.6%		9.6%		49.6%		18.5%		7.2%	
red-sequence	55.3%		26.1%		25.1%		51.3%		21.6%		8.4%	
sSFR	29.6%		8.6%		14.4%		43.5%		9.4%		2.5%	
photo-SED	44.7%		14.4%		11%		41.4%		10.9%		2.6%	
pure passive	25.2%		7%		5.2%		38.9%		3.2%		1.6%	
<b>presence of emission lines</b>												
morphology	-32.6	62.7%	-12.3	34.9%	-13.3	35.5%	-24.6	74%	-11.3	42.8%	-9.1	32.9%
UVJ	-14.0	42.1%	-10.8	26.6%	-10.1	28.7%	-16.5	46.2%	-10.7	41.7%	-9.2	37.9%
red-sequence	-14.3	41.8%	-11	33.8%	-10.9	36.3%	-13.4	39.2%	-10.5	43.3%	-9.2	38.5%
sSFR	-12.0	20.7%	-9.4	25.9%	-10.4	31.4%	-13.4	14.1%	-8.3	21.2%	-8.4	26.6%
photo-SED	-12.2	30.4%	-9.2	27.8%	-9.5	28.9%	-8.6	10.75%	-7.9	21.6%	-8.3	23%
pure passive	–	–	–	–	–	–	–	–	–	–	–	–
<b>non-elliptical morphology</b>												
morphology	–	–	–	–	–	–	–	–	–	–	–	–
UVJ	2.1	60.6%	2.1	31%	2.1	15.2%	2.1	67.3%	2.1	52.7%	2.1	29.9%
red-sequence	2.1	60.8%	2.1	39%	2.1	22.8%	2.1	67.2%	2.1	55.4%	2.1	31.5%
sSFR	2.1	50.2%	2.1	31.4%	2.1	18.6%	2.1	63%	2.1	45.7%	2.1	23.7%
photo-SED	2.1	51.9%	2.1	30%	2.1	18.9%	2.1	59.6%	2.1	44.8%	2.1	22.9%
pure passive	2.1	34.8%	2.1	25.7%	2.1	11.3%	2.1	77.8%	2.1	40.7%	2.1	15.1%

**Table 2.** Contamination of the different ETGs samples as a function of stellar mass and redshift. The table reports the median values of colors, sSFR, equivalent widths and morphology for the galaxies having blue colors, high specific star formation rates, significant emission lines and late-type morphologies as defined in Sect. 4.1, and the percentage relative to each subsample. The low-mass bin refers to  $\log(\mathcal{M}/\mathcal{M}_{\odot}) < 10.25$ , the med-mass bin to  $10.25 < \log(\mathcal{M}/\mathcal{M}_{\odot}) < 10.75$ , and the high-mass bin to  $\log(\mathcal{M}/\mathcal{M}_{\odot}) > 10.75$ . As defined in the text, the emission lines reported are the median restframe equivalent widths (in units of  $\text{\AA}$ ) of H $\alpha$  for  $z \leq 0.5$  and of [OII] for  $z > 0.5$ ; by convention, the emission lines are quoted with negative values.

percentage of contamination in both optical colors ( $\lesssim 5\%$ ), IRAC colors ( $\lesssim 15\%$ ), spectroscopic features ( $\lesssim 30\%$ ) and sSFR ( $\lesssim 15\%$ ). The percentage of contamination is slightly higher than the “pure passive” criterion, on average by a factor of  $\sim 2$ , but the absolute values of the properties of contaminants are still compatible with a red, passively evolving population.

#### 4.4. Number density

For all the ETGs samples, we estimated the galaxy stellar mass functions using the non-parametric  $1/V_{\text{max}}$  formalism (Schmidt, 1968), from which we derived the number density ( $\rho_N$ ) in three mass bins,  $\log(\mathcal{M}/\mathcal{M}_{\odot}) = 10.25 - 10.75, 10.75 - 11, 11 - 11.5$ . The redshift evolution of the galaxy number density is shown

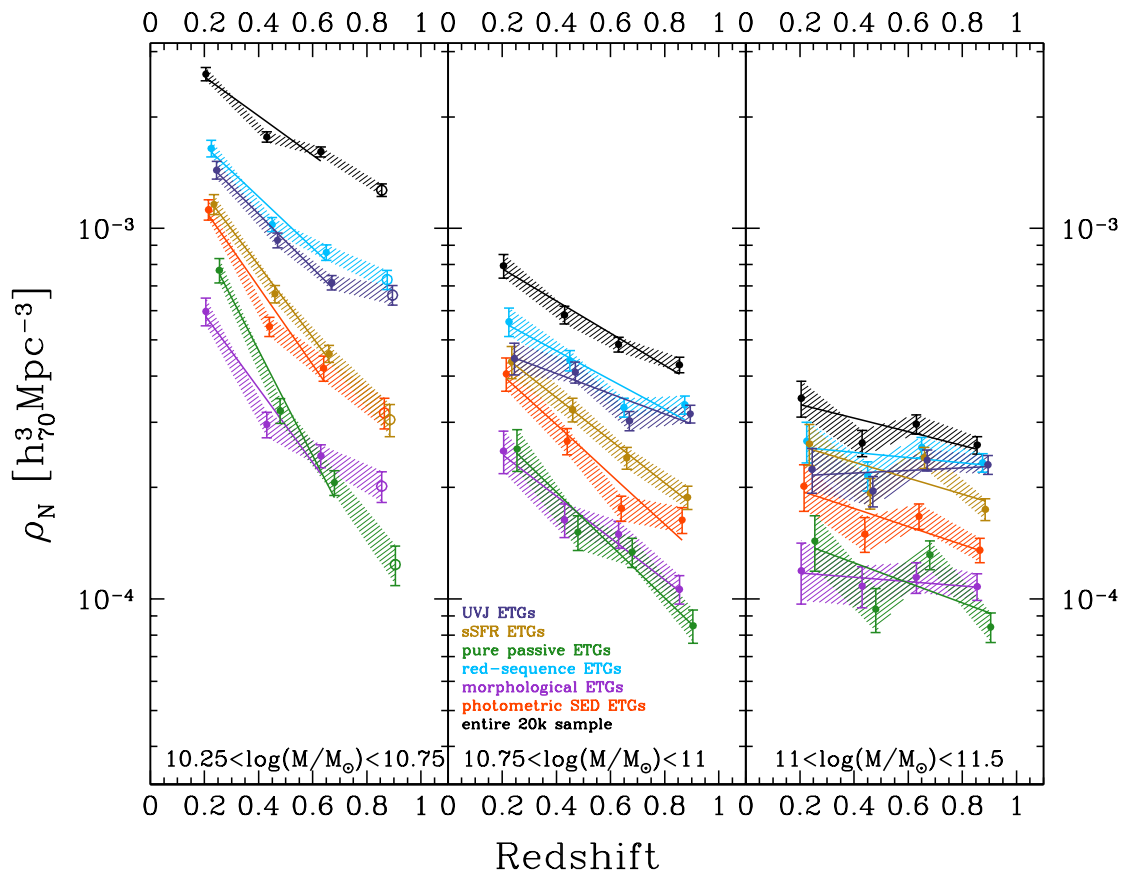


**Fig. 12.** Redshift evolution of the galaxy number density, derived using  $1/V_{\max}$ , for three different mass ranges:  $10.25 < \log(\mathcal{M}/M_{\odot}) < 10.75$  (left panel),  $10.75 < \log(\mathcal{M}/M_{\odot}) < 11$  (central panel) and  $\log(\mathcal{M}/M_{\odot}) > 11$  (right panel). The different colors represent different selection criteria (violet for the “morphological” ETGs, blue for the “UVJ” ETGs, cyan for the “red-sequence” ETGs, yellow for the “sSFR” ETGs, orange for the “photometric SED” ETGs, and green for the “pure passive” ETGs). The lines represent the fit to the observed  $\log(\rho_N(z))$  relation. The open points represent the lower limits where the survey is not complete.

in Fig. 12. As a comparison, we reported also the number density in the same mass range for the parent zCOSMOS-20k sample. Each relation has been fitted using a weighted linear least square minimization, considering only the redshift bins in which the data are complete. The trends are similar for the differently selected ETGs, even if the normalization is different.

In the lower stellar mass bin, we find a pronounced evolution, with an increase in number densities by a factor  $\sim 2 - 4$  between  $z \sim 0.65$  and  $z \sim 0.2$ . At stellar masses  $10.75 < \log(\mathcal{M}/M_{\odot}) < 11$  we still find a noticeable evolution, with an increase by a factor  $\sim 2-3$  between  $z \sim 0.85$  and  $z \sim 0.2$ . At higher masses,  $11 < \log(\mathcal{M}/M_{\odot}) < 11.5$ , the evolution is much less pronounced, with a percentage increase in number density of  $\sim 10-50\%$  in the entire redshift range.

The stronger increase in the number density of low/intermediate-masses ETGs with respect to massive ETGs is a clear indication of mass-assembly downsizing (Fontana et al., 2004; Drory et al., 2005; Bundy et al., 2006; Cimatti et al., 2006; Thomas et al., 2010; Pozzetti et al., 2010; Moresco et al., 2010), with more massive galaxies having assembled their mass at higher redshifts and being already in place at  $z \sim 1$ . This result

of this analysis is in agreement with many other works: Scarlata et al. (2007) studying ETGs in the COSMOS field found no traces of significant evolution in the number density of bright ( $\sim L > 2.5L^*$ ) ETGs, with a maximum increase of  $\sim 30\%$  from  $z \sim 0.7$  to  $z \sim 0$  when allowing for different star formation histories and cosmic variance; Pozzetti et al. (2010) found an almost negligible evolution in the number density of quiescent galaxies in zCOSMOS-10k sample,  $< 0.1$  dex between  $z = 0.85$  and  $z = 0.25$  for  $\log(\mathcal{M}/M_{\odot}) > 11 - 11.5$ ; Ilbert et al. (2013) from the analysis of the UltraVISTA-DR1 sample found that massive galaxy ( $\log(\mathcal{M}/M_{\odot}) > 11.2$ ) do not show any significant evolution between  $0.8 < z < 1.1$  and  $0.2 < z < 0.5$ , while low-mass ones ( $\log(\mathcal{M}/M_{\odot}) \sim 9.5$ ) increase in number density by a factor  $> 5$ . Brammer et al. (2011) analyzed the number density of quiescent galaxies at  $0.4 < z < 2.2$  using the NEWFIRM Medium-Band Survey, and found a strong evolution of  $\log(\mathcal{M}/M_{\odot}) > 10.5$  galaxies, a factor  $\sim 10$  from  $z \sim 2$  to  $z \sim 0$ ; however, this evolution becomes smaller and comparable with the errorbars at high masses between  $z \sim 1$  and  $z \sim 0.6$ , only  $\sim 20\%$  for  $\log(\mathcal{M}/M_{\odot}) > 11$  ( $\sim 10\%$  for  $10.6 < \log(\mathcal{M}/M_{\odot}) < 11$ ), therefore being compatible with our results. Maraston et al. (2012), studying the stellar mass function of BOSS galaxies,

find that the galaxy number density above  $\sim 2.5 \cdot 10^{11} M_{\odot}$  agrees with previous measurements within 2 sigma, with no evolution detected from  $z \sim 0.6$ . Finally, Moustakas et al. (2013) measured the evolution of the stellar mass function from the PRISM Multi-object Survey, and confirmed an evolution by a factor of  $3.2 \pm 0.5$  from  $z = 0.4$  to  $z = 0$  for stellar masses  $9.5 < \log(\mathcal{M}/M_{\odot}) < 10$ , by a factor of  $2.2 \pm 0.4$  from  $z = 0.6$  to  $z = 0$  for stellar masses  $10 < \log(\mathcal{M}/M_{\odot}) < 10.5$ , and only  $\sim 58\% \pm 9\%$  for stellar masses  $10.5 < \log(\mathcal{M}/M_{\odot}) < 11$ .

It is interesting also the comparison, at fixed mass, of the number density of the differently selected ETGs, since it sheds some lights on the time-scales characteristic of different processes. At masses  $\log(\mathcal{M}/M_{\odot}) < 11$  we find that the number densities of the various samples are well separated, with the highest normalization for color-selected ETGs, intermediate for the sSFR/photometric SED selected ETGs, and the lowest for the morphologically selected ETGs: this may suggest a scenario for which at these masses the first transition and ETGs experience is a color transformation from blue to red, then the star formation is completely quenched, and finally the morphological transformation takes place.

This picture is confirmed also by the work of Pozzetti et al. (2010), which quantified the timescale of the delay between color and morphological transformation to be around 1-2 Gyr. Another confirmation for this scenario comes from the work of Ilbert et al. (2010), who find that the stellar mass density of quiescent galaxies is always higher than the one of red elliptical galaxies. Obviously the quantitative estimate of the delay between these processes depends also on the adopted cuts to select ETGs, since e.g. a lower/higher cut in sSFR will shift the relation lower/higher.

#### 4.5. Revising the color selection criteria

In Sect. 3.1 and 4.1 we have presented and discussed the fact that the “red-sequence” and the “UVJ” are the samples with an higher contamination, clearly evident also by a visual inspection of the color-mass and color-color diagrams. However, we have also argued that this higher contamination may be due to the fact that the proposed cut may be not optimal, at least for the zCOSMOS-20k survey.

To address this issue, we decided to study how the colors of the contaminants (as defined in Sect. 4.1) for these two criteria are distributed in the  $(U - B)_{\text{rest}}$  color-mass and UVJ color-color diagrams respectively, to understand if an additional cut is able to further reduce the contamination. In Fig. 13 we show the  $(U - B)_{\text{rest}}$ -mass diagram for the “red-sequence” ETGs (in gray), highlighting in cyan the galaxies presenting a sSFR or emission lines in excess with respect to the “passive” cuts defined (i.e. the *contaminants*); Fig 14 shows the same as Fig. 13, but for the  $(U - V)_{\text{rest}}-(V - J)_{\text{rest}}$  diagram and for the case of the “UVJ” ETGs. From these plots it is evident that statistically the contaminants have bluer colors, and therefore that a refined cut may help to reduce the contamination. In particular from Fig. 14 it is clear that there are specific ranges of colors ( $1.3 < (U - V)_{\text{rest}} < 1.5$ ) where the contaminants represent the 100% of the distribution.

We therefore defined two revised color selection criteria, with slightly redder colors. For the  $(U - B)_{\text{rest}}$ -mass

diagram:

$$(U - B)_{\text{rest}} > 1.15 + 0.075 \times \log\left(\frac{\mathcal{M}}{10^{10} M_{\odot}}\right) - 0.18 \times z$$

and for the  $(U - V)_{\text{rest}}-(V - J)_{\text{rest}}$  diagram

$$\begin{cases} (U - V)_{\text{rest}} > 1.6 \\ (V - J)_{\text{rest}} > 1.6 \\ (U - V)_{\text{rest}} > 0.88 * (V - J)_{\text{rest}} + 0.69 \end{cases} [0 < z < 0.5]$$

$$\begin{cases} (U - V)_{\text{rest}} > 1.5 \\ (V - J)_{\text{rest}} > 1.6 \\ (U - V)_{\text{rest}} > 0.88 * (V - J)_{\text{rest}} + 0.66 \end{cases} [0.5 < z < 1]$$

The empty colored histograms in Figs. 13 and 14 show the distribution of the contaminants with the old definitions, while the shaded colored histograms show the distribution of the contaminants obtained with the new definitions just reported. It is evident how these new color selection criteria help to cut significantly the contaminants with blue colors.

We checked that these new selection criteria provide purer ETG samples than the previous ones. The new “UVJ” sample does not present anymore significant blue tails in the color-mass diagram, having a contamination compatible with all the other samples; as well the percentage of contamination of the new “red-sequence” sample in the UVJ color-color diagram is reduced from 20-40% to 15-25% at low redshift and from 20-40% to 10-15% at high redshift. Even if reduced, however also with these new definitions the contamination in terms of sSFR and presence of emission lines is still higher than the “sSFR”, “photometric SED”, and “pure passive” criteria, which continue to behave better than the color criteria in selecting a purer sample of ETGs.

## 5. Summary and conclusions

We have studied the photometric, spectroscopic and morphological properties of 6 differently selected samples of ETGs, to analyze their contamination in terms of blue/star-forming/non-passive galaxies. From the zCOSMOS-20k spectroscopic catalog, we extracted a sample based on morphology (2421 “morphological” early-type galaxies), on optical colors (4894 “red-sequence” and 4886 “UVJ” early-type galaxies), on specific star formation rate (2937 “sSFR” early-type galaxies), on a best-fit to the observed SED (2603 “photometric SED” early-type galaxies), and on a criterion which combines morphological, spectroscopic and photometric information (1530 “pure passive” early-type galaxies).

We estimated for all the samples, the  $(U - B)_{\text{rest}}$ -stellar mass diagram, the IRAC color-color plot as defined by Lacy et al. (2004), the sSFR- $\text{EW}_0([\text{OII}]/\text{H}\alpha)$  diagram, and the morphological types. We have also evaluated the median stacked spectra of these samples, to search in detail for the presence of peculiar spectroscopic features which may be a proxy of star formation activity.

To quantify the contamination of the various samples, for each property we defined an “early-type” cut and studied the percentage of galaxies not fulfilling this cut, as well as the median value of the parameters (color, sSFR,  $\text{EW}_0$  of emission lines) involved in each selection: in this way we were able to study also how much these contaminants

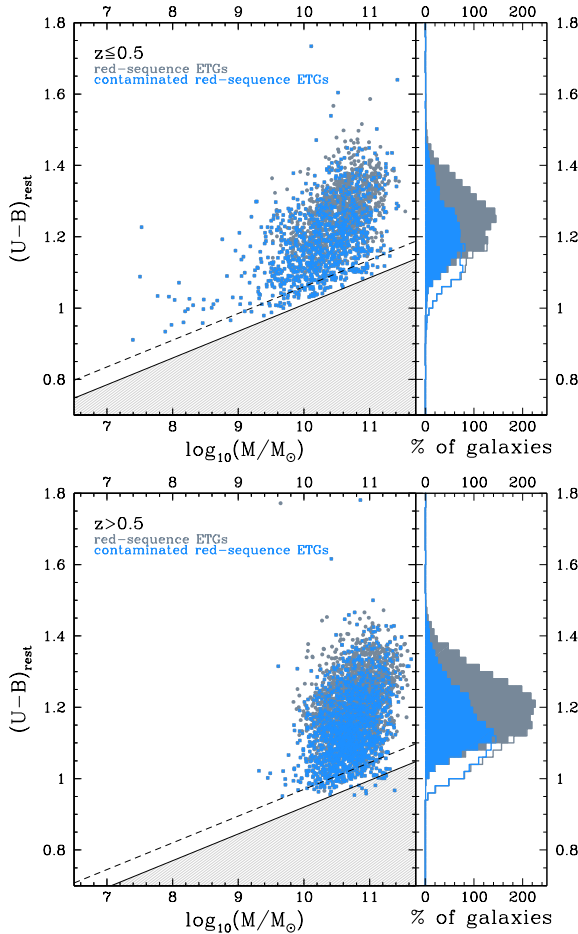


**Fig. 13.**  $(U - B)_{\text{rest}}$ -mass diagram. In grey is shown the original  $(U - B)_{\text{rest}}$ -mass criterion as defined by Peng et al. (2010), and in cyan are highlighted the galaxies presenting a sSFR or emission lines in excess with respect to the “passive” cuts. The empty cyan histograms show the distribution of the contaminants with the old definitions, while the shaded cyan histograms the distribution of the contaminants with the new selection criterion as defined in section 4.5. The upper plot shows the diagram obtained for  $z \leq 0.5$ , and the lower plot for  $z > 0.5$ .

are close to or far from the assumed “early-type” definition. All these analyses were performed in two redshift bins ( $z \leq 0.5$  and  $z > 0.5$ ) and three stellar mass bins ( $\log(\mathcal{M}/\mathcal{M}_{\odot}) < 10.25$ ,  $10.25 < \log(\mathcal{M}/\mathcal{M}_{\odot}) < 10.75$ , and  $\log(\mathcal{M}/\mathcal{M}_{\odot}) > 10.75$ ).

Our main results are listed below:

- We find that all samples display tails in the star-forming regions of different diagrams, irrespectively of the severity of the criterion adopted. This contamination has been shown to be dependent on the stellar mass for all the samples, with more massive samples being less biased than low massive ones. This fact demonstrates that a cut in stellar mass is helpful to improve the purity of the sample.
- The comparison between the different selection criteria shows that the best performing is the one based on a combined selection, since it takes into account all the available information about the galaxies (morphologi-

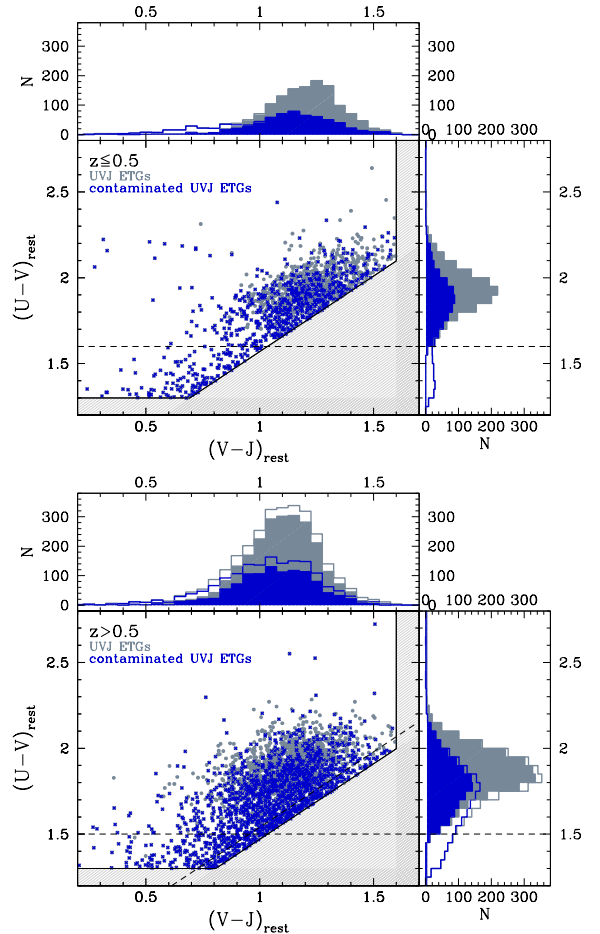


**Fig. 14.**  $(U - V)_{\text{rest}}-(V - J)_{\text{rest}}$  diagram. In grey is shown the original UVJ criterion, as defined by Williams et al. (2009), and in blue are highlighted the galaxies presenting a sSFR or emission lines in excess with respect to the “passive” cuts. The empty blue histograms show the distribution of the contaminants with the old definitions, while the shaded blue histograms the distribution of the contaminants with the new selection criterion as defined in section 4.5. The upper plot shows the diagram obtained for  $z \leq 0.5$ , and the lower plot for  $z > 0.5$ .

cal, spectroscopic and photometric), with the obvious disadvantage of being highly demanding in terms of the data needed. For this sample, we find that the contamination is minimized, especially for stellar masses  $\log(\mathcal{M}/\mathcal{M}_{\odot}) > 10.25$ :  $<10\%$  for both optical and IRAC colors,  $\lesssim 10\%$  in sSFR and with weak emission lines equivalent widths for the contaminants ( $\lesssim 10 \text{ \AA}$ ).

- The “morphological” criterion is the one with the larger contamination, and a high percentage of blue, emission-lines, star-forming elliptical galaxies has been found in this sample ( $\sim 20\text{--}70\%$ , depending on the mass range). Among the other selection criteria, we identify the “photometric SED” and the “sSFR” to be the best ones, since they trade a slight increase in contamination (about a factor 2) with the fact that they are extremely economic in terms of information required.
- The slope of the number density as a function of redshift at fixed mass for the various samples is

similar: we found an increase in number density in the mass range  $10.25 < \log(M/M_{\odot}) < 10.75$  from  $z = 0.65$  to  $z = 0.2$  by a factor  $\sim 2$ -4, in the mass range  $10.75 < \log(M/M_{\odot}) < 11$  from  $z = 1$  to  $z = 0.2$  by a factor  $\sim 2$ -3, while for massive ETGs  $11 < \log(M/M_{\odot}) < 11.5$  this increase from  $z = 1$  to  $z = 0.2$  is only  $\sim 10$ -50% (and  $< 10\%$  between  $z = 1$  and  $z = 0.4$ ). This trend in mass confirms that most massive ETGs are already in place at  $z \sim 1$ . The comparison of the different number densities supports a scenario for which in ETGs we have first the color transformation from blue to red, followed by the quenching of the star formation, and concluded by the morphological transformation from late-type to ellipticals.

- By analyzing the color-mass and color-color diagrams, we proposed two revised selection criteria, which help to reduce the contamination by blue star-forming galaxies.

Selecting a sample of ETGs the less contaminated as possible by star-forming objects is crucial for an unbiased study of the properties of this population of galaxies. The analysis presented in this paper provides a first detailed comparison of the contamination obtained with different ETG selection criteria, and represents an important step forward the identification of the best ways of selecting ETGs. This will be fundamental especially for the new and upcoming surveys such as BOSS (Schlegel et al., 2009) and Euclid (Laureijs et al., 2011) that will provide the scientific community an unprecedented statistic of these objects, in particular at high redshift. From this point of view, this work represents the starting point to study and develop optimized ETG selection criteria also at  $z > 1$ , to be applied e.g. to Euclid simulations.

In a forthcoming paper we aim to study how much the different selections presented here affect the study of the evolution of early-type galaxies.

*Acknowledgements.* MM and AC acknowledge the grants ASI n.I/023/12/0 “Attività relative alla fase B2/C per la missione Euclid” and MIUR PRIN 2010-2011 “The dark Universe and the cosmic evolution of baryons: from current surveys to Euclid”. Part of the work has been supported also by an INAF grant “PRIN-2010”.

## References

- Annibali F., Bressan A., Rampazzo R., et al., 2010, *A&A*, 519, A40  
 Aviles A., Bravetti A., Capozziello S., et al., 2013, *PhRvD*, 87, 044012  
 Baldry I. K., Glazebrook K., Brinkmann J., et al., 2004, *ApJ*, 600, 681  
 Baldry I. K., Balogh M. L., Bower R., et al., 2004, *AIPC*, 743, 106  
 Baldry I. K., Balogh M. L., Bower R. G., et al., 2006, *MNRAS*, 373, 469  
 Baldry I. K., Glazebrook K., Driver S. P., 2008, *MNRAS*, 388, 945  
 Baldwin J. A., Phillips M. M., Terlevich R., 1981, *PASP*, 93, 5  
 Balogh M., Eke V., Miller C., et al., 2004, *MNRAS*, 348, 1355  
 Bell E. F., Wolf C., Meisenheimer K., et al., 2004, *ApJ*, 608, 752  
 Brammer G. B., Whitaker K. E., van Dokkum P. G., et al., 2011, *ApJ*, 739, 24  
 Brinchmann J., Charlot S., White S. D. M., et al., 2004, *MNRAS*, 351, 1151  
 Bruzual G., Charlot S., 2003, *MNRAS*, 344, 1000  
 Bundy K., Ellis R. S., Conselice C. J., et al., 2006, *ApJ*, 651, 120  
 Calzetti D., Armus L., Bohlin R. C., et al., 2000, *ApJ*, 533, 682  
 Capak P., Aussel H., Ajiki M., et al., 2007, *ApJS*, 172, 99  
 Chabrier G., 2003, *PASP*, 115, 763  
 Cimatti A., Daddi E., Renzini A., 2006, *A&A*, 453, L29  
 Coleman G. D., Wu C.-C., Weedman D. W., 1980, *ApJS*, 43, 393  
 Donley J. L., Koekemoer A. M., Brusa M., et al., 2012, *ApJ*, 748, 142  
 Drory N., Salvato M., Gabasch A., et al., 2005, *ApJ*, 619, L131  
 Eisenstein D. J., Annis J., Gunn J. E., et al., 2001, *AJ*, 122, 2267  
 Fontana A., Pozzetti L., Donnarumma I., et al., 2004, *A&A*, 424, 23  
 Franzetti P., Scoddeggio M., Garilli B., et al., 2007, *A&A*, 465, 711  
 Garilli B., Fumana M., Franzetti P., et al., 2010, *PASP*, 122, 827  
 Heckman T. M., 1980, *A&A*, 87, 152  
 Hogg D. W., Blanton M., Strateva I., et al., 2002, *AJ*, 124, 646  
 Ilbert O., Arnouts S., McCracken H. J., et al., 2006, *A&A*, 457, 841  
 Ilbert O., Capak P., Salvato M., et al., 2009, *ApJ*, 690, 1236  
 Ilbert O., Salvato M., Le Fèvre O., et al., 2010, *ApJ*, 709, 644  
 Ilbert O., McCracken H. J., Le Fèvre O., et al., 2013, *arXiv*, arXiv:1301.3157  
 Jimenez R., Loeb A., 2002, *ApJ*, 573, 37  
 Kauffmann G., Heckman T. M., White S. D. M., et al., 2003, *MNRAS*, 341, 54  
 Kinney A. L., Calzetti D., Bohlin R. C., et al., 1996, *ApJ*, 467, 38  
 Koekemoer A. M., Aussel H., Calzetti D., et al., 2007, *ApJS*, 172, 196  
 Lacy M., Storrie-Lombardi L. J., Sajina A., et al., 2004, *ApJS*, 154, 166  
 Lamareille F., Contini T., Le Borgne J.-F., et al., 2006, *A&A*, 448, 893  
 Laureijs R., Amiaux J., Arduini S., et al., 2011, *arXiv*, arXiv:1110.3193  
 Le Fèvre O., Saisse M., Mancini D., et al., 2003, *SPIE*, 4841, 1670  
 Le Fèvre O., Vettolani G., Garilli B., et al., 2005, *A&A*, 439, 845  
 Lilly S. J., Le Fèvre O., Renzini A., et al., 2007, *ApJS*, 172, 70  
 Lilly S. J., Le Brun V., Maier C., et al., 2009, *ApJS*, 184, 218  
 Maraston C., Pforr J., Henriques B. M., et al., 2012, *arXiv*:1207.6114  
 Masters K. L., Maraston C., Nichol R. C., et al., 2011, *MNRAS*, 418, 1055  
 Meneux B., Le Fèvre O., Guzzo L., et al., 2006, *A&A*, 452, 387  
 Mignoli M., Zamorani G., Scoddeggio M., et al., 2009, *A&A*, 493, 39  
 Moresco M., Pozzetti L., Cimatti A., et al., 2010, *A&A*, 524, A67  
 Moresco M., Jimenez R., Cimatti A., et al., 2011, *JCAP*, 3, 45  
 Moresco M., Cimatti A., Jimenez R., et al., 2012, *JCAP*, 8, 6  
 Moresco M., Verde L., Pozzetti L., et al., 2012, *JCAP*, 7, 53  
 Moustakas J., Coil A., Aird J., et al., 2013, *arXiv*, arXiv:1301.1688  
 Peng Y.-j., Lilly S. J., Kováč K., et al., 2010, *ApJ*, 721, 193  
 Phillips M. M., Jenkins C. R., Dopita M. A., et al., 1986, *AJ*, 91, 1062  
 Polletta M., Tajer M., Maraschi L., et al., 2007, *ApJ*, 663, 81  
 Pozzetti L., Bolzonella M., Zucca E., et al., 2010, *A&A*, 523, A13  
 Renzini A., 2006, *ARA&A*, 44, 141  
 Riemer-Sørensen S., Parkinson D., Davis T. M., et al., 2013, *ApJ*, 763, 89  
 Said N., Baccigalupi C., Martinelli M., et al., 2013, *arXiv*, arXiv:1303.4353  
 Scarlata C., Carollo C. M., Lilly S. J., et al., 2007, *ApJS*, 172, 406  
 Scarlata C., Carollo C. M., Lilly S. J., et al., 2007, *ApJS*, 172, 494  
 Schlegel D., White M., Eisenstein D., 2009, in *Astronomy*, Vol. 2010, astro2010: The Astronomy and Astrophysics Decadal Survey, p. 314  
 Schmidt M., 1968, *ApJ*, 151, 393  
 Scoddeggio M., Franzetti P., Garilli B., et al., 2005, *PASP*, 117, 1284  
 Scoville N., Aussel H., Brusa M., et al., 2007, *ApJS*, 172, 1  
 Simon J., Verde L., Jimenez R., 2005, *PhRvD*, 71, 123001  
 Stern D., Jimenez R., Verde L., et al., 2010, *JCAP*, 2, 8  
 Strateva I., Ivezić Ž., Knapp G. R., et al., 2001, *AJ*, 122, 1861  
 Silva L., Granato G. L., Bressan A., et al., 1998, *ApJ*, 509, 103  
 Thomas D., Maraston C., Schawinski K., et al., 2010, *MNRAS*, 404, 1775  
 Tully R. B., Mould J. R., Aaronson M., 1982, *ApJ*, 257, 527  
 Tasca L. A. M., Kneib J.-P., Iovino A., et al., 2009, *A&A*, 503, 379  
 Visvanathan N., Sandage A., 1977, *ApJ*, 216, 214  
 Wang X., Meng X.-L., Zhang T.-J., et al., 2012, *JCAP*, 11, 18  
 Williams R. J., Quadri R. F., Franx M., et al., 2009, *ApJ*, 691, 1879  
 Yan R., Newman J. A., Faber S. M., et al., 2006, *ApJ*, 648, 281  
 Yan R., Blanton M. R., 2012, *ApJ*, 747, 61  
 Zehavi I., Zheng Z., Weinberg D. H., et al., 2011, *ApJ*, 736, 59  
 Zucca E., Ilbert O., Bardelli S., et al., 2006, *A&A*, 455, 879  
 Zucca E., Bardelli S., Bolzonella M., et al., 2009, *A&A*, 508, 1217

<sup>1</sup> Dipartimento di Fisica e Astronomia, Università degli Studi di Bologna, V.le Berti Pichat, 6/2 - 40127, Bologna, Italy

<sup>2</sup> INAF – Osservatorio Astronomico di Bologna, via Ranzani 1, I-40127, Bologna, Italy

<sup>3</sup> Institut de Recherche en Astrophysique et Planétologie, CNRS, F-31400 Toulouse, France

<sup>4</sup> Institute for Astronomy, ETH Zurich, 8093 Zurich, Switzerland

<sup>5</sup> IRAP, Université de Toulouse, UPS-OMP, Toulouse, France

<sup>6</sup> Laboratoire d'Astrophysique de Marseille, Aix Marseille Université, CNRS, 13388, Marseille, France

<sup>7</sup> European Southern Observatory, Garching, Germany

<sup>8</sup> INAF – Osservatorio Astronomico di Padova, Padova, Italy

<sup>9</sup> INAF – Istituto di Astrofisica Spaziale e Fisica Cosmica, Milano, Italy

<sup>10</sup> INAF – Osservatorio Astronomico di Roma, 00040, Monteporzio Catone, Italy

<sup>11</sup> Institute for Astronomy, The University of Edinburgh, Royal Observatory, Edinburgh, EH93HJ, UK

<sup>12</sup> INAF – Osservatorio Astronomico di Brera, Milano, Italy

<sup>13</sup> Space Telescope Science Institute, Baltimore, MD 21218, USA

<sup>14</sup> Institute for the Physics and Mathematics of the Universe, 5-1-5 Kashiwanoha, 277-8583 Kashiwa, Japan

<sup>15</sup> INAF – Istituto di Astrofisica Spaziale e Fisica Cosmica, Bologna, Italy

<sup>16</sup> Institute for Astronomy, University of Hawaii, 2680 Woodlawn Drive, Honolulu, HI 96822, USA

<sup>17</sup> Institut d'Astrophysique de Paris, Université Pierre & Marie Curie, 75014 Paris, France

<sup>18</sup> UC Santa Cruz/UCO Lick Observatory, 1156 High Street, Santa Cruz, CA 95064, USA

<sup>19</sup> Minnesota Institute for Astrophysics, School of Physics and Astronomy, University of Minnesota, Minneapolis, MN 55455, USA

<sup>20</sup> California Institute of Technology, MC 249-17, 1200 East California Boulevard, Pasadena, CA 91125, USA

<sup>21</sup> Institut d'Astrophysique Spatiale, Batiment 121, CNRS & Univ. Paris Sud XI, 91405 Orsay Cedex, France

<sup>22</sup> Centro de Estudios de Física del Cosmos de Aragón, Plaza San Juan 1, planta 2, 44001, Teruel, Spain

<sup>23</sup> Kapteyn Astronomical Institute, University of Groningen, P.O. Box 800, 9700 AV Groningen, The Netherlands

<sup>24</sup> University of Vienna, Department of Astrophysics, Tuerkenschanzstrasse 17, 1180 Vienna, Austria